Cui, Linfan; Yliniemi, Kirsi; Vapaavuori, Jaana; Lundström, Mari

Recent developments of electrodeposition-redox replacement in metal recovery and functional materials: A review

Published in:
Chemical Engineering Journal

DOI:
10.1016/j.cej.2023.142737

Published: 01/06/2023

Document Version
Publisher's PDF, also known as Version of record

Please cite the original version:
Cui, L., Yliniemi, K., Vapaavuori, J., & Lundström, M. (2023). Recent developments of electrodeposition-redox replacement in metal recovery and functional materials: A review. *Chemical Engineering Journal*, *465*, Article 142737. https://doi.org/10.1016/j.cej.2023.142737

Chemical Engineering Journal 465 (2023) 142737

Contents lists available at ScienceDirect

Chemical Engineering Journal

journal homepage: www.elsevier.com/locate/cej

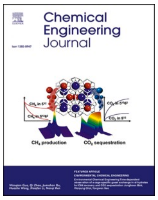

Review

Recent developments of electrodeposition-redox replacement in metal recovery and functional materials: A review

Linfan Cui [a,b], Kirsi Yliniemi [b], Jaana Vapaavuori [b], Mari Lundström [a,*]

[a] *Department of Chemical and Metallurgical Engineering, School of Chemical Engineering, Aalto University, Espoo 02105, Finland*

[b] *Department of Chemistry and Materials Science, School of Chemical Engineering, Aalto University, Espoo 02105, Finland*

ARTICLE INFO

Keywords:
Metal recycling
Electrochemical recovery
Hydrometallurgy
Low-grade raw materials
Noble metals deposition

ABSTRACT

One way to overcome the complex problem of the increasing demand for metals coupled with the rapid depletion of high-grade raw materials is to boost research into innovative methods of metal recovery. Electrochemical recovery for metal production has already gained ground in the electrowinning and electrorefining of Cu, Zn, and Au, for example, from highly concentrated and purified hydrometallurgical solutions. Since 2015, an electrochemical technique, based on the combination of the electrodeposition (ED) and redox replacement (RR) processes, has been developed in the context of trace metal recovery (μg/L – mg/L). Specifically, EDRR enables the efficient recovery of precious metals, including Ag, Au, Pt, and Te, from underutilized secondary raw materials-hydrometallurgical solutions, where these metal species are naturally present. With highly flexible electrochemical process parameters, EDRR also allows controllable preparation of metal coatings, nanoparticles, and even functional surfaces directly from lower-grade resources, further indicating the promise of EDRR to relieve material scarcity. In this review, we analyze in detail the significant progress regarding EDRR for both metal recovery behavior and creation of high-value-added materials. The future prospects for EDRR, including energy efficiency and sustainable materials, are also outlined.

1. Introduction

Metal scarcity has become an impending concern due to the depletion of the world's natural resources. It is predicted that many of the supplies of primary metals (e.g., Ag, Pb, Cu, Zn) will reach their production peak soon and several metals will be depleted within approximately 50 years [1–12]. However, metal-containing products are widely utilized in housing, transportation, electrical power production and delivery, contributing to modern technology and quality of life. From the perspective of the environment, metal materials are also irreplaceable in sustainable technologies to phase out fossil fuels, such as solar panels, wind turbines, electric vehicles, and H_2 fuel cells [13]. For example, the consumption of Pt in the automotive industry for catalytic converters is up to 100 t per year depending on the Pt load per unit of power, and the required amount of Pt in fuel cell technology is continuously increasing [14]. The high demand for metals and metal-containing products necessitates efficient metal extraction and recycling techniques.

Hydrometallurgical processing methods, such as leaching, precipitation, cementation, and electrochemical reduction, have served as industrial methods for the metal refining [15]; for example, cyanide leaching for Au processing has been developed in the industry for >100 years [16]. Electrochemical recovery of metals was first employed to obtain Na metal by the electrolysis of molten sodium hydroxide in 1807 [17] and has become the dominant technology in elemental metal recovery from concentrated and purified solutions. Metals are either purified by electrochemical leaching-deposition (electrorefining, ER) from their pyrometallurgically smelted metal anodes (for Cu, Ni, Co, Pb, Sn, etc.) [18] or recovered by electrodeposition (electrowinning, EW) after hydrometallurgical leaching and solution purification processes (for Cu, Au, Ag, Zn, Al, Ni, Co, Mn, etc.) [19]. Solutions for EW are usually concentrated, for example, the industrial EW of Cu operates typically in a 20–50 g L^{-1} solution [20,21] and that of Ni in a 90–140 g L^{-1} solution [22,23]. When applying traditional EW in dilute metal solutions, the

---

Abbreviations: PGMs, platinum group metals; ER, electrorefining; EW, electrowinning; EDRR, electrodeposition-redox replacement; PLS, pregnant leaching solution; SLRR, surface-limited redox replacement; SPR, surface plasmon resonance; OCP, open circuit situation; CV, cyclic voltammetry; ChCl, $(CH_3)_3NC_2H_4OHCl$; EG, 1,2-ethanediol $HOCH_2CH_2OH$; SEM, scanning electron microscope; OPEX, operating expenditure.

* Corresponding author.

E-mail address: mari.lundstrom@aalto.fi (M. Lundström).

https://doi.org/10.1016/j.cej.2023.142737
Received 20 December 2022; Received in revised form 25 March 2023; Accepted 31 March 2023

hindered mass transfer, i.e., movement of metal ions from the solution to the electrode surface has an influence on the recovery time. Frequently, adaptation of the equipment (e.g., an electrode with a larger surface area or rapid flow) and operating parameters (e.g., higher operating current density) is required [24–26]. Moreover, the purity of metals recovered by EW is limited in solutions with impurities, such as those in industrial process streams. It is worth noting that the global annual production of Cu, Ni, and Zn (26 Mt, 2.7 Mt, and 13 Mt, respectively, in 2021) [27] is mainly refined from hydrometallurgical or pyro-hydrometallurgical operations. In the final stage, these process solutions still contain impurities, such as precious metals Ag, Au, and PGM, at very low concentrations (<mg L^{-1} or <μg L^{-1}) [22,28–30]. Considering the depletion of high-grade raw materials, such hydrometallurgical process solutions and production side streams provide great potential as secondary raw materials for further metal recovery. Currently the recovery from such low concentrations (<mg L^{-1} or <μg L^{-1}) is not considered economically feasible, the development of new recycling methods is significant and necessary.

Electrodeposition-redox replacement (EDRR) has recently been developed for metal recovery from process solutions, specifically for precious metals [31–33]. During EDRR, a short current or potential is first applied to achieve the electrodeposition (ED) of a less noble/sacrificial metal (Cu, Ni, Zn), which is present in hydrometallurgical solutions at high concentrations (g L^{-1} scale), analogously to the EW process. In the subsequent step, no electricity is applied, and more noble metals present in dissolved form (μg L^{-1} – mg L^{-1} levels) are recovered through a spontaneous redox replacement (RR) reaction, driven by the differences in reduction potential or galvanic potential between the two metals, similarly to the cementation process.

Compared to traditional hydrometallurgical processes (Table 1) [140], such as cementation, precipitation, solvent extraction and ion exchange, no additional chemicals or pH adjustment is required in EDRR. Moreover, electrochemical processes (e.g., EW and EDRR) are expected to be more viable options in future as the share of renewable electricity in the energy mix is rising, allowing the use of these methods to decrease overall carbon emissions in metal production as well. Both electrochemical methods are highly controllable by the selected operation parameters, i.e., deposition current or potential and deposition time, whereas for example cementation is a batch process allowing no control after the addition of cementation agents. EDRR has additional parameters in RR step, making it more flexible to achieve optimized purity of recovered metals. Furthermore, neither the concentration nor purification steps of the solution are necessary before the EDRR process. Another extra benefit of EDRR is that the dissolution of sacrificial metals during each RR step increases their concentration near the electrode (replenishing process), which not only compensates for the possible mass-transport limitation in the following ED step (cf. EW), but the same metal atoms can be continuously used for target metal reduction without additional cementation agents. During the process of EDRR, the double layer charging takes place in the beginning of each cycle and its role in energy consumption cannot be ignored, while the double layer charging in EW only happens at the very start of the process. EW is a strong candidate in the industrial metal recovery which present at high concentrations (g L^{-1}). Although the recover limit of EW on lab scale reached even 5–100 mg L^{-1} [34–37], higher energy is consumed in such dilute solution due to the mass transfer limitation. The actual metal recovery of EDRR takes place during RR step where no external energy is applied, and therefore EDRR shows great potential in the recovery of metals which are present at low concentrations (even < μg L^{-1}) either in the primary or recycled process solutions.

To date, EDRR has been effectively applied for metal extraction and removal on laboratory scale, including Ag recovery from a Zn- and Cu-containing dilute effluent or hydrometallurgical bottom ash leachant [38–41], Au recovery from cyanide-free cupric chloride leaching solution [42–44], Pt recovery from industrial Ni solution [22], and Te recovery from Doré slag pregnant leaching solution (PLS) [45,46].

From the viewpoint of materials science, the cycling of the electrodeposition and redox replacement process was originally studied for the fabrication of metal nanoparticle deposition (e.g., Pt/Pb) [47]. Other redox replacement reactions, such as surface-limited redox replacement (SLRR) [48,49], based on underpotential deposition and electroless adsorption driven by galvanic displacement, have been developed as prominent methods to create defect-free and smooth monolayer films of precious metals (e.g., Ag, Au, Pt, Pd) [50]. However, the SLRR process requires a solution with a more optimized ratio of sacrificial and replacement metal species and proceeds under specific conditions, such as deoxygenation [51]. In comparison, EDRR can be operated easily under ambient conditions and functional metal products with highly controllable properties can be created directly from hydrometallurgical process solutions, further benefitting the circular economy. Thus far, versatile metal deposition such as Ni/Pt, Ag/Zn, Ag/Cu, Cu/Zn, Cu/Zn/Ag [52–57] has been obtained using EDRR. In particular, Ni/Pt has proved to be efficient for photocatalytic H_2 evolution and holds great promise in the hydrogen economy to support decarbonization [52]; Ag/Zn and Ag/Cu have exhibited surface plasmon resonance (SPR) behavior, which has become a widely growing optical sensing approach

Table 1
Comparison of EDRR with commonly used hydrometallurgical processes.

	EDRR	EW	Cementation	Precipitation (crystallization)	Solvent extraction	Ion exchange
Addition of extra chemicals (cost of chemicals)	**No**	**No**	Yes (Moderate)	Yes (Moderate)	Yes (High)	Yes (High)
Adjustment of pH (effect of pH)	**No**	Sometimes	Yes	Yes (Solubility of metal salts varies at different pH)	Yes (Extraction and selectivity are pH dependent)	Yes (Extraction and selectivity are pH dependent)
Recovery by electricity (energy consumption)	**Yes** (Low in complex and dilute solution)	**Yes** (Low in concentrated solution)	No	No	No	No
Recovery of metal or metal salts directly from solution without additional unit process	**Yes**	**Yes**	**Yes**	**Yes**	No (Metals are recovered into other phases)	No (Metals are recovered into other phases)
High selectivity and purity of target metals from complex and impure solution	**Yes**	No	No	No	**Yes**	**Yes**
Utilization of low-grade raw materials-process solution (concentration scale)	**Yes** (<1 μg L^{-1} or <1 mg L^{-1})	No (g L^{-1})	No (g L^{-1})	Yes (mg L^{-1}- g L^{-1})	No (g L^{-1})	Yes (mg L^{-1} - g L^{-1})
Technology readiness level	Moderate	High	High	High	High	High

[55,57]; Cu/Zn has also exhibited corrosion resistant properties [56,57].

Development of the EDRR method would greatly advance the integration of metal recovery and material functionalization, aligning well with the principles of the circular economy and sustainable development (Fig. 1). In this review, we give a comprehensive introduction to the EDRR technique, including the general process and mechanism. Applications of EDRR for metal recovery/removal and direct deposition of functional materials are also discussed. Finally, we outline the future prospects for EDRR.

2. Fundamentals of electrodeposition-redox replacement (EDRR)

EDRR methodology includes two electrochemical processes, i.e., electrodeposition and redox replacement. In terms of hydrometallurgy, EDRR can be considered as an electrochemically assisted form of cementation or a combination of EW and cementation (Fig. 2).

2.1. Electrodeposition process

The principle of electrodeposition is the cathodic reduction of metal ions, producing a solid deposit on the cathode within an electrolytic cell (Fig. 2, electrowinning) [58]. Reduction occurs when the applied potential is more negative than the equilibrium potential of specific metal/metal ion pairs in a non-standard state, which can be determined by the Nernst equation:

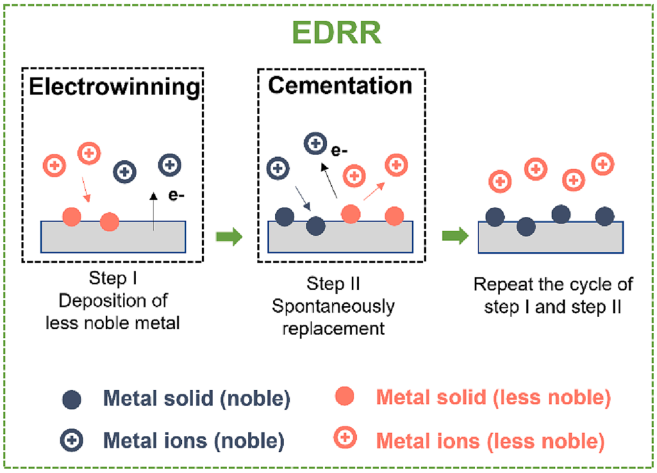

Fig. 2. Schematic of the EDRR process.

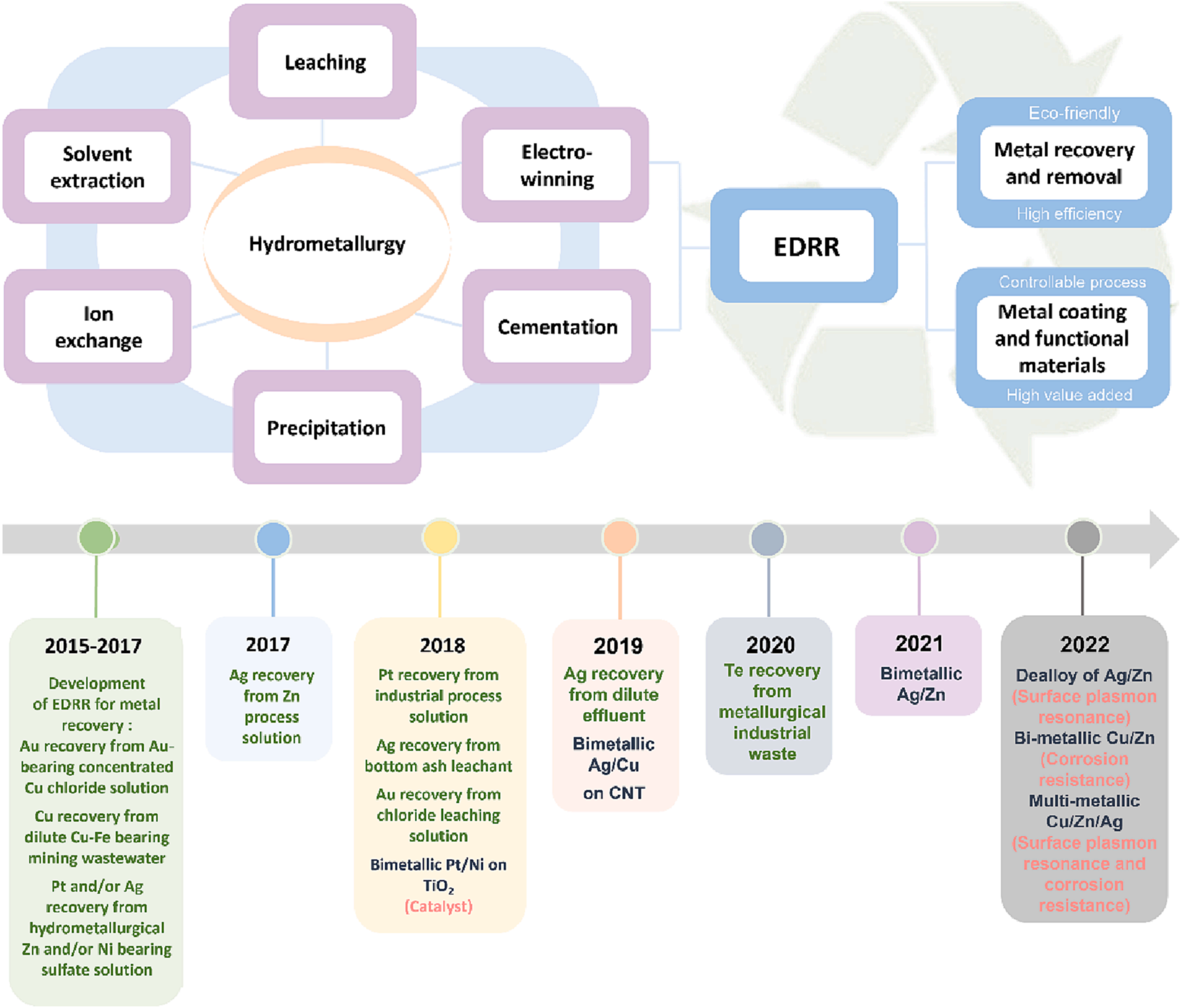

Fig. 1. Development of EDRR for metal recovery and production from hydrometallurgical solutions.

$$E = E^{o} + RT/zF\ln a_{Mz+} \quad (1)$$

where E is the electrode potential, E° is the standard reduction potential for a specific metal/metal ion, R represents the universal gas constant, z is the charge on the metal ion, F represents the Faraday constant, with the activity of metal ion a_{Mz+} and absolute temperature T. The differences of standard reduction potentials between various species theoretically enable the selective deposition of the target metal from a complex multi-metallic solution (Table 2) [59]. For example, in ideal cases, dissolved Ag is more noble (+0.799 V vs SHE) and can be separated from dissolved Cu (+0.34 V vs SHE), whereas dissolved Cu can also be selectively separated from Zn (-0.763 V vs SHE). If the deposition potentials of metals are more negative than the H_2 reduction potential (Table 2), H_2 evolution may compete with the electrodeposition. During an industrial ER process, the metal to be purified acts as the anode, whereas the pure target metal is deposited on the cathode, making the thermodynamical cell potential 0 V. In an industrial EW process, cathodic reduction is for the recovery of the elemental target metal, while the anodic reaction is typically O_2 evolution in sulfate-based media or Cl_2 evolution in chloride-based solutions, making a substantially higher cell potential when compared to ER [15].

2.2. Cementation process

In a hydrometallurgical cementation process, one of the dissolved metals with a higher electrode potential will be reduced to zero valence by the metallic particles with a lower electrode potential (Fig. 2, Table 2) [60]. The method allows the recovery (spontaneous reduction) of dissolved metals from the leaching solution, by adding cementation agents (typically Zn and Fe) in metallic form. For instance, Zn powder is used to recover Au from cyanide solutions in industrial processes (the so-called Merrill-Crowe process) [61,62]. Cementation has also been widely applied for the purification of leaching solutions to remove metals such as Cu and Co from solutions where these impurity metals are typically present in relatively low amounts (<1 g L^{-1}) [63–65].

2.3. EDRR process and parameters

EDRR parameters are highly amenable to being tailored, allowing easier optimization of metal recovery, and flexible adjustment of the composition and structure of the metal deposition. During the ED step (Fig. 3), a constant or pulsed deposition potential ($\boldsymbol{E_1}$) or cathodic current ($\boldsymbol{i_1}$) is applied to the electrode for a certain deposition time ($\boldsymbol{t_1}$). In the RR step, the system is left in an open circuit situation (OCP) without the application of external potential or current. During this step, the OCP value increases due to the replacement on the electrode of a less noble metal with a more noble metal. The RR step can be allowed to continue until the OCP reaches a predetermined cut-off potential ($\boldsymbol{E_2}$) or cut-off time ($\boldsymbol{t_2}$), whichever is reached first or determined as the controlling parameter (Fig. 3). When each full EDRR cycle is completed, the next one will start without delay and the cycling ($\boldsymbol{n}$) of ED and RR is repeated (Fig. 3).

Table 2
Examples of standard reduction potentials.

Electrode	Reduction half reaction	Standard reduction potential (V)
$Au^+\|Au$	Au^+ (aq) + e^- → Au (s)	+1.83
$Cl_2\|Cl^-$	Cl_2 (g) + 2e^- → 2Cl^- (aq)	+1.40
$O_2\|H_2O$	O_2 (g) + 4H^+ (aq) + 4e^- → 2H_2O (l)	+1.23
$Pt^{2+}\|Pt$	Pt^{2+} (aq) + 2e^- → Pt (s)	+1.20
$Ag^+\|Ag$	Ag^+ (aq) + e^- → Ag (s)	+0.80
$Fe^{3+}\|Fe^{2+}$	Fe^{3+} (aq) + e^- → Fe^{2+} (aq)	+0.77
$O_2\|H_2O_2$	O_2 (g) + 2H^+ (aq) + 2e^- → H_2O_2 (l)	+0.70
$Te^{4+}\|Te$	Te^{4+} (aq) + 4e^- → Te (s)	+0.57
$Cu^{2+}\|Cu$	Cu^{2+} (aq) + 2e^- → Cu (s)	+ 0.34
$Cu^{2+}\|Cu^+$	Cu^{2+} (aq) + e^- → Cu^+ (g)	+0.16
H^+/H_2	H^+ (aq) + e^- → ½ H_2 (g)	0
$Ni^{2+}\|Ni$	Ni^{2+} (aq) + 2e^- → Ni (s)	−0.23
$Zn^{2+}\|Zn$	Zn^{2+} (aq) + 2e^- → Zn (s)	−0.76

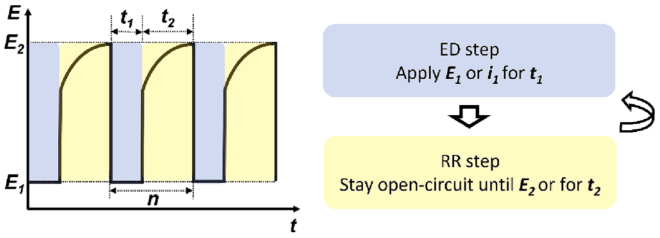

Fig. 3. Schematic of a typical EDRR process with parameters.

The range of $\boldsymbol{E_1}$ **or** $\boldsymbol{i_1}$ depends on the redox behavior of the sacrificial and noble metal pairs in the solutions, which can be defined through experimental study of cyclic voltammetry (CV) characteristics (Fig. 4, light red area in CV: selected range of $\boldsymbol{E_1}$). A more negative deposition potential $\boldsymbol{E_1}$ (or higher cathodic i_1) or longer $\boldsymbol{t_1}$ typically results in a higher sacrificial metal content; side reactions such as H_2 evolution may occur in acidic or neutral solutions, accompanied by higher energy consumption.

The $\boldsymbol{E_2}$ or $\boldsymbol{t_2}$ in the RR reaction is typically adjusted to allow all the deposited sacrificial metals to be replaced by noble metals. In practice, the duration of the RR step varies from microseconds to several hours. More positive $\boldsymbol{E_2}$ or longer $\boldsymbol{t_2}$ will lead to higher purity of the end-product, due to the increased dissolution of the sacrificial metals [52] and more migration of metal ions toward the electrode, especially in solutions with trace noble metals (μg L^{-1} – mg L^{-1}). However, the cut-off potential should not exceed the reduction potential of the noble metal (determined by CV in Fig. 4) to prevent its stripping, i.e., corrosion.

In general, operating more EDRR cycles leads to increased metal recovery, as long as there are still target noble metals present in the solution. The number of cycles can also be adjusted to control the deposit size and coverage, e.g., Ostwald ripening occurs with a longer EDRR process time, leading to bigger crystalline particles [66]. With more EDRR cycles, individually distributed particles tend to form a continuous layer due to their surface energy and the mobility of metal atoms [67–69].

The recovery efficiency and the obtained structures of the metal deposits are not only dependent on the EDRR parameters, but subject to the mass transfer and selection of sacrificial metals. In addition to the metal concentration in solution, the mass transfer is also influenced by the EDRR parameters or agitation process applied. The selection of sacrificial metal usually depends on the metal species present and their redox potentials in hydrometallurgical solutions. The solutions in the hydrometallurgical industry are usually chloride-, sulfate- or nitrate-based, resulting in both the complexation and variation of the metals' redox potentials (compared to their standard potentials, Table 2). Generally, the reduction potentials of the sacrificial metal and recovered metal should not overlap, and thus their nobility difference enables the RR reaction to occur. In theory, the larger the reduction potential difference between the sacrificial metal and recovered metal, the bigger the driving force for the RR reaction [70]. It should be noted, however, that utilizing a sacrificial metal with a more negative reduction potential causes a higher cell voltage during the ED step and increases the energy consumption accordingly.

3. EDRR for metal recovery

EDRR has been studied in the context of hydrometallurgy for the recovery of various metals either from synthetic or industrial process solutions tested on laboratory scale (Table 3). It is evident that the

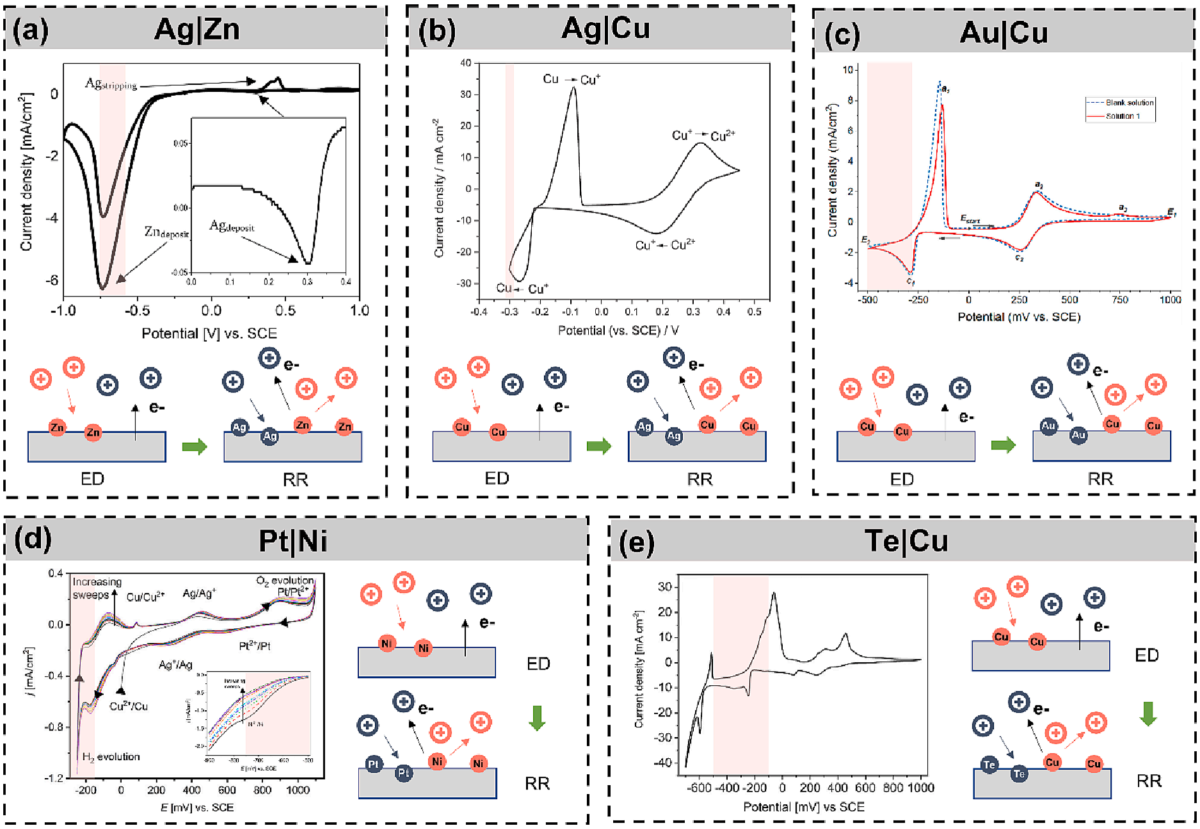

Fig. 4. EDRR processes applied to different metal pairs, including the cyclic voltammetry (CV) measurements and schematics of metal recovery. The shaded area in the CVs shows the potential regions applicable for the deposition potential E_1. a) Ag|Zn. Reproduced with permission [38]. Copyright 2017, American Chemical Society. b) Ag|Cu. Reproduced with permission [39]. Copyright 2018, Taylor & Francis. c) Au|Cu. Reproduced with permission [42]. Copyright 2018, Elsevier. d) Pt|Ni. Reproduced with permission [22]. Copyright 2018, American Chemical Society. e) Te|Cu. Reproduced with permission [45]. Copyright 2020, Springer Nature.

recovery of various metals displays different behavior, which will be discussed in detail in the following sections.

3.1. Ag recovery

Ag-based products are attractive in diverse fields, including optics, catalysis, electronics, and anti-bacteria [72–75]. In general, Ag is obtained as a by-product from production of Zn, Cu, Ni metals, or along with precious metal production such as that of Au [76–78]. Ag recovery from multi-metal industrial process solutions typically includes several steps, such as separation from the leach solution via solvent extraction, ion exchange, adsorption and/or the recovery from solution by cementation, precipitation, or EW [79]. The precipitates formed can be further purified by the above-mentioned unit processes and/or smelting.

The EDRR method has demonstrated its capability to recover Ag directly from hydrometallurgical process solutions [38–41,53,54]; both Zn and Cu were found to be successful sacrificial metals for Ag recovery in sulfate- or chloride-based media. In concentrated Zn sulfate solution (Zn: 60 g L^{-1}), Zn(II) was deposited on the electrode in the ED step ($\boldsymbol{E_1}$ = -0.7 V, Fig. 4a), followed by spontaneous replacement with Ag(I) (Ag: 100 mg L^{-1}, difference in reduction potential between Zn^{2+}/Zn and Ag^{+}/Ag of approximately 1.6 V) [38]. By optimizing the EDRR parameters, the deposited layer contained Ag of high purity. The Ag:Zn ratio was around 1500:1, which was 20 times higher than Ag enrichment through EW (Ag:Zn ratio = 230:11), indicating the superior performance of EDRR. However, H_2 reduction as well as Zn corrosion were evident during the ED step, consuming most of the applied current and resulting in a charge efficiency (the electrical charge consumed during the ED compared to that of Ag stripping) of only 13 % [38]. However, when Cu served as the sacrificial metal ($\boldsymbol{E_1} = -0.3$ V, Fig. 4b) in a HCl-based bottom ash leach solution, no competing H_2 evolution occurred [39].

3.2. Au recovery

Cyanide leaching is one of the most common hydrometallurgical processes for large-scale Au extraction from ore and is generally followed by adsorption methods (carbon-in-leach or resin-in-leach) applied to the leaching solution to achieve further recovery of Au [80–83]. However, the cyanide-containing processes have a hazardous impact on both the environment and human health [84]. Several precious metal plants also operate with chloride-based media during Au refining [85], and hence cyanide-free and chloride-based processes are under development [86–90]. A special characteristic of chloride-based media is the ability to stabilize dissolved Au and Cu complexes (e.g., monovalent Cu chloride complex).

The recovery of Au in minor quantities from cupric chloride leaching solution by EDRR has been studied, where Cu is the sacrificial metal (Fig. 4c) [42–44]. EDRR enabled effective metal enrichment, demonstrated by the increased ratio of Au:Cu from 1:340 (in the initial solution) to 3.3:1 (in the final product on the electrode), when applying EDRR in a solution containing 175 g L^{-1} NaCl, 1.2 g L^{-1} Cu, and 100 mg L^{-1} Au [42]. The energy consumption was 114.3 kWh kg^{-1} when recovering 8.4 % Au [42], indicating comparable performances of EDRR with EW at low Au concentrations (e.g., 112 kWh kg^{-1} in 5 mg L^{-1} Au cyanide solution) [34,91,92]. Moreover, EDRR exhibited higher current efficiency (40 % in 8 mg L^{-1} Au solution), as the value was generally <1 % in EW (e.g., 10 mg L^{-1} Au solution) [35,93], suggesting the benefit of the RR step in EDRR. However, lower energy consumption (e.g., 5–15 kWh kg^{-1}) can be obtained by EW at higher Au concentrations (e.g., 100

Table 3
Summary of the EDRR results for metal recovery.

Recovered metal| sacrificial metal (Year)	Recovery solution	Media	Investigated parameters	Recovery limit	Recovery result	Ref. No.
Ag|Zn (2017)	Synthetic Zn process solution: **Zn: 60 g/L** H_2SO_4: 10 g/L **Ag: 1 μg/L –250 mg/L**	Sulfate	**E_1**: −0.75, −0.70, −0.65 V vs SCE **t_1**: 2–40 s **E_2**: 0.25, 0.3, 0.35 V vs SCE **n**: 10–160	1 μg L^{-1} –250 mg L^{-1}	Ag on the electrode: 69 wt% Ag:Zn ratio in the final product: 1500 Ag:Zn ratio in the initial solution: 0.0017	[38]
Ag|Cu + Zn (2018)	Lab-scaled bottom ash leach solution: Ca: 13.8 g/L, Al: 4.7 g/L, **Cu: 2.5 g/L, Zn: 1.2 g/L**, Fe: 1.2 g/L, S: 1 g/L, Mg: 0.8 g/L, P: 0.5 g/L, Pb: 0.2 g/L, **Ag: 3.5 mg/L** Synthetic solutions: **Cu: 2.5 g/L, Zn: 1.2 g/L, Ag: 10 mg/L**	Chloride	**E_1**: −0.3 V vs SCE **t_1**: 5, 10, 15 s **E_2**: 0.3 V vs SCE **t_2**: 1000 s **n**: 10	3.5 mg L^{-1}	Ag vs (Cu + Zn) ratio on electrode: 0.3Ag vs (Cu + Zn) ratio in initial solution: 6.8×10^{-5}	[39]
Ag|Zn (2019)	Synthetic Zn process solution: **Zn: 60 g/L** H_2SO_4: 10 g/L $Fe_2(SO_4)_3$: 0–1000 mg L^{-1} **Ag: 100 mg/L**	Sulfate	**E_1**: −1600, −1500 mV **t_1**: 1, 2.5, 5, 10, 20 s **E_2**: −100 mV **n**: 100, 40, 20, 10, 5 (total deposition time: 100 s)	100 mg L^{-1}	Ag on the electrode: 83 ± 2 wt % Ag:Zn ratio in the final product: 20.1 Energy consumption: ~8.5 kWh kg^{-1}	[40]
Ag|Cu (2021)	Synthetic Cu process solution: H_2SO_4: 49 g/L **Cu: 320 mg/L** **Ag: 5.4 mg/L**	Sulfate	**E_1**: − 0.1 V vs Ag/AgCl **t_1**: 0.2 s **t_2**: 5, 10 s **n**: last about 427 s	5.4 mg L^{-1}	Pure Ag on the electrode	[41]
Au|Cu (2018)	Synthetic Au process solution: NaCl: 120–175 g/L **Cu: 1.2–2.7 g/L** **Au: 8–100 mg/L**	Chloride	**E_1**: −500, −475, −375, −320, −300, −275 mV vs SCE **t_1**: 1, 5, 10, 20 s **E_2**: 0, 300, 550, 600 mV vs SCE **n**: 10, 20, 250	8–100 mg L^{-1}	Au:Cu ratio in the final product: 3.3:1 Au:Cu ratio in the initial solution: 1:340 Energy consumption: 114.3 kWh kg^{-1}	[42]
Au|Cu (2019)	Lab-scaled Au leach solution: **Cu: 30 g** L^{-1}, **Au: 1.2 mg** L^{-1}, Fe: ~1 g L^{-1}, Co < 20 mg L^{-1}, Ni < 20 mg L^{-1}, Zn < 20 mg L^{-1}, Pb < 20 mg L^{-1}, Na:11.9 g L^{-1}, Ca: 11.9 g L^{-1}, Mg: 32 mg L^{-1}, Al: 37 mg L^{-1}, K: 77 mg L^{-1}	Chloride	**E_1**: −350 mV vs SCE **t_1**: 10 **t_2**: 30 s **n**: 2500	1.2 mg L^{-1}	Au on the electrode: >99 wt% Energy consumption: 2.3 kWh kg^{-1}	[43]
Au|Cu (2020)	Synthetic Au process solution (aqueous) NaCl: 263 g L^{-1}, **$CuCl_2·2H_2O$: 10.2 g** L^{-1}, HCl: 364.6 mg L^{-1}, **Au: 98.5 mg/L**Synthetic Au process solution (deep eutectic solutions) : **Au: 98.5 mg/L**, **Cu: 10.2 g/L,** Cl: 170.2 g/L	Chloride	Aqueous solution: **E_1**: −0.35 V vs Ag/AgCl ChCl: EG: **E_1**: −0.35 V vs Ag/AgCl **t_1**: 10 **t_2**: 600 **n**: 50	98.5 mg L^{-1}	Au on the electrode: 94 wt% (aqueous solution), 14 wt% (aqueous solution) Energy consumption: 11.6 kWh kg^{-1} (aqueous solution), 9.7 kWh kg^{-1} (deep eutectic solution)	[44]
Pt|Ni + Cu + Ag (2018)	Synthetic Ni process solution: **Ni: 60 g** L^{-1}, H_2SO_4: 10 g L^{-1}, **Pt: 20 mg** L^{-1}, Ag: 10 mg L^{-1}, Cu: ~1 mg L^{-1}, Industrial base metal process solution: #1: **Ni: 141–141 g** L^{-1}, Ag: 5.9 μg L^{-1}, **Pt:** < limit of detection, Fe: 16 g/L, Cu: 6 g/L #2: **Ni: 141–141 g** L^{-1}, Ag: < limit of detection, **Pt:** < limit of detection, Fe: 4.2 mg L^{-1}, Cu: <limit of detection	Sulfate	**E_1**: −750, −500, −175 V vs SCE **t_1**: 2, 5, 8, 10 s **E_2**: 175 mV vs SCE **t_2**: 1000 s **n**: 10, 100, 200, 400	< limit of detection-20 mg L^{-1}	Pt on the electrode: 98 wt% (synthetic solution), 90 wt% (industrial solution #1), 85 wt % (industrial solution #2) Pt: Ni + Cu + Ag ratio in the final product: 33.6:1 (synthetic solution) Pt: Ni + Cu + Ag ratio in the initial solution: 3×10^4 (synthetic solution) Enrichment of Pt: 10^5 (synthetic solution), 7.6×10^{10} (industrial solution #1),7.2×10^{10} (industrial solution #2)	[22]
Te|Cu (2020)	Lab-scaled Doré slag leach solution: Bi: 4.6 g/L, **Cu: 3.9 g/L**, Fe: 1.4 g/L, Na, Ba, As, B, and Pb: 1.4–6.4 g/L, **Te: 421 mg/L**		**E_1**: −500, −300, −100, +100, −50, +50, +150 mV vs SCE **t_1**: 2 s **E_2**: −50, +50, +150 mV vs SCE **t_2**: 1000 s **n**: 100	421 mg L^{-1}	Te on the electrode: 64 wt%	[45]
Te|Cu (2021)	Lab-scaled Doré slag leach solution: Bi: 4.6 g/L, **Cu: 3.9 g/L**, Fe: 1.4 g/L, **Te: 100–500 mg/L**	Chloride	**E_1**: −500 mV vs SCE **t_1**: 2 s **E_2**: 150 mV vs SCE **t_2**: 1000 s **n**: 100	100–500 mg L^{-1}	Te on the electrode: 80 wt% Energy consumption: 40 kWh kg^{-1}	[46]

(*continued on next page*)

Table 3 (*continued*)

Recovered metal|sacrificial metal (Year)	Recovery solution	Media	Investigated parameters	Recovery limit	Recovery result	Ref. No.
Recovered metals (Year)	Raw material	Recovery method	Operation time	Recovery result		Ref. No.
Te (2020)	Lab-scaled Doré slag leach solution: Bi: 4.6 g L^{-1}, Cu: 3.9 g L^{-1}, Fe: 1.4 g L^{-1}, Na, Ba, As, B, and Pb: 1.4–6.4 g L^{-1}, Te: 421 mg L^{-1}	EW + EDRR	96 h (EW) + 96 h (EDRR)	Te on the electrode: 37 wt%		[45]
Au (2022)	PLS of ground telluride gold ore: Solids concentration: 200 g/L, Au: > 1 mg L^{-1}	Cupric chloride leaching + filtration + EDRR + precipitation	150 h (14 rounds of the leaching-EDRR process, 8 h for leaching in each stage)	Au content in the final product: 58.2 % Au:Cu ratio in the final product: 1.4 Au:Cu ratio in the initial solution: 3.5×10^{-5} Enrichment factor of Au: 40 000 Energy consumption: 31.4 kWh kg^{-1} in the first stage, 10–15 kWh kg^{-1} in the following rounds		[71]

mg L^{-1}) [35]. Hence, EDRR is typically targeted at solutions containing only minor amounts of the metals to be recovered. From an industrial chloride leaching solution tested on laboratory scale (1.2 mg L^{-1} Au, 30400 mg L^{-1} Cu with other chemical compositions, Na, Ca, Fe, Co, Ni, Zn, Pb, Mg, Al, K), the purity of recovered Au reached over 99 wt% [43].

Beside the aqueous solutions discussed above, the EDRR process was also studied in a deep eutectic mixture of chloride solution ($(CH_3)_3NC_2H_4OHCl$, ChCl) with ethylene glycol (1,2-ethanediol $HOCH_2CH_2OH$, EG). In comparison, a higher selectivity of Au recovery was achieved in aqueous solution due to the higher mass transfer (the Au purity was 94 wt% from aqueous solution, 14 wt% from ChCl:EG) [44]. The energy consumption of the EDRR process was similar in two types of solution, i.e., 11.6 kW h kg^{-1} in aqueous solution and 9.7 kWh kg^{-1} in 1:2 ChCl:EG; these values are in the range of state-of-the art industrial process [94].

It was also indicated for the first time that Au reduction may occur via aqueous reduction close to the electrode surface [44]. Specifically in chloride-based media, the reduction of a $CuCl_2$ complex to a $CuCl_3^{2-}$ complex was shown to occur, and the reduced aqueous species triggered the consequent Au(I) deposition on the electrode during the RR step, indicating that the actual electrodeposition into metallic form is not indispensable in EDRR [54]. In ChCl:EG, a similar process was observed but with hindered kinetics due to the limited ionic conductivity.

3.3. *Pt recovery*

As a precious metal, Pt is scarce in the Earth's crust [95]. In conventional hydrometallurgy, Pt is a side product of the fabrication of Ni, Co, or Zn and is typically removed as a mixture of noble metals, which needs further purification in dedicated noble metal refineries [22,96,97]. EDRR has demonstrated the unique feature of recovering minute amounts of Pt in hydrometallurgical Ni process solutions (Fig. 4d) [22,52]. Again, the competing evolution of H_2 occurs when the applied $\boldsymbol{E_1}$ is more negative than its onset potential.

When applying EDRR in industrial solutions (Ni: >140 g L^{-1}, Pt: <1 µg L^{-1}, Pd: <117 µg L^{-1}, Ag: <4 µg L^{-1}), the deposited electrode surface was found to contain ~90 wt% Pt with a Pt/Ni enrichment ratio of 10^{11} [22]. The content of Pt recovered by EDRR increased 2- to 10-fold when compared to EW for the same electrodeposition potential and equal deposition time, indicating the effectiveness of EDRR when applied for lower-grade raw resources [22]. In addition to Ni, elements such as Cu and Ag also served as sacrificial metals when enough $\boldsymbol{t_1}$ was applied to allow their co-deposition, while precious metals such as Pd and Ag were obtained on the electrode before being fully replaced by Pt by controlling the $\boldsymbol{t_2}$ or $\boldsymbol{n}$ during RR [22]. As illustrated by this example, EDRR displays its flexibility in controlling the recovered species by means of parameter adjustment.

3.4. *Te recovery*

Tellurium is a rare metal element in the Earth's crust, with a content of approximate 1 µg L^{-1} [98]. It is commonly applied in semiconductors, thermoelectrics, mechanic alloying, and CdTe solar panels with increasing demand [99–105]. The primary source of Te is the side product of the ER process for Cu. Conventional routes to recover Te combine hydro- and pyrometallurgical processes, e.g., pressure leaching from anode slime under an acidic and/or alkaline environment [106]. However, minute amounts of Te remain in the slime after these industrial recovery processes and subsequent application of EDRR can prevent the loss of Te, enhancing both the environmental and economic sustainability of Te production. Only a few studies have addressed the recovery of Te from solutions containing several hundred mg L^{-1} of Te [107,108]. Tellurium recovery by EDRR was shown to be possible from mg L^{-1}-level Te-containing solutions, such as PLS derived from the aqua regia leaching of industrial Doré slag (contains Na, B, Ba, Bi, Cu, Pb, Fe, Mg, Al, Sb, etc.) [45,46].

To demonstrate Te recovery by EDRR, Cu was selected as the sacrificial element, as the deposition potentials do not overlap in chloride-based solutions (Cu: ~ −150 mV vs SCE, Te: ~350 mV vs SCE) [45]. It is worth noting that the reduction potential of Cu decreases in chloride-based solutions due to the stability of monovalent Cu complexes [109]. Tellurium also exhibits various oxidation stages in electrolytes, depending on the pH and the presence of various elements [110,111]. The possible Te species in 30 % aqua regia medium are Te^{4+} ions or $TeCl_6^{2-}$ complexes, leading to a wide range of reduction potentials (Fig. 4e, selection of $\boldsymbol{E_2}$: −50, +50, +150 mV vs SCE) [45,112]. In complex Te-containing solutions, co-deposition of other metallic impurities is inevitable during the electrodeposition process; the metals co-deposited during the ED step also act as sacrificial elements, which are eventually replaced by more noble elements, i.e., Te dissolved in the solution.

In the work of Halli et al., 64 wt% Te was obtained by EDRR from PLS (Te: 421 mg L^{-1}) with a total electrodeposition time of only 200 s, whereas the Te content was only 55 wt% after 1200 s deposition within the EW process, indicating the mass-transport limitation of EW in a dilute solution [45]. Impurities such as Cu, Bi, and Sb are also co-deposited with Te during EW, affecting the recovery purity [113–115]. In conventional Te EW, the concentration of Te in industrial solutions is on the g L^{-1} scale [116], and the energy consumption of Te EW at a concentration of, for example, 35–350 g L^{-1} was 1.3–2.7 kWh kg^{-1} [37,113,117,118]. Although the energy consumption of EDRR was an order of magnitude higher than that of EW (14–63 kWh kg^{-1}), the Te to be recovered in the solution was only from 500 to 100 mg L^{-1} [101].

3.5. Side reactions during EDRR

In real industrial solutions with a complex multi-metal matrix, side reactions of the impurities occur as well (Fig. 5a), which affect the whole EDRR process, such as recovery amount, purity, and energy consumption. Among all the impurities, Fe is a typical multivalent species present in hydrometallurgical processes [22,40,43]. For instance, the stainless-steel fragments of battery casings usually accumulate in the leaching solution during battery crushing-sieving pretreatment [40]. In both EDRR and EW, the presence of Fe impurities causes extra energy consumption due to the reduction of Fe(III) species to Fe(II) species at the cathode: the higher the concentration of ferric species, the more energy consumption and lower current efficiency for metal recovery [40,119]. It worth noting that EDRR is more energy efficient when the concentration of Fe(III) is lower than 100 mg L^{-1}, and the energy consumption was 2.5 kWh kg^{-1} at a Fe(III) concentration of 10 ppm (EW: approximately 8 kWh kg^{-1} when Ag is 100 mg L^{-1}). Hence the energy efficiency for Ag recovery by EDRR is competitive, even in comparison with recovery from a nonferrous solution, where the energy consumption of Ag EW was 4.56 kWh kg^{-1} (500 mg L^{-1} Ag) [25], 0.8 kWh kg^{-1} (1 g L^{-1} Ag) [120], and 1 kWh kg^{-1} (3 g L^{-1} Ag) [121]. However, EDRR consumes more energy than EW in a solution with a high concentration of Fe(III) (over 500 mg L^{-1}), indicating that EDRR may have an energy efficiency limit in such solutions on industrial scale [40]. Moreover, the competing Fe(III)/Fe(II) reduction during the ED step causes less deposition of sacrificial metals, which also decreases the final yield of recovered noble metal [119]. On the other hand, dissolved Fe(III) species could have a positive effect on the purity of the recovered metal during EDRR, even at a low Fe concentration: as in a sulfate-based Ag solution, the Fe(III) species oxidize the deposited Zn as well, resulting in higher Ag purity (Fig. 5a) [40]. The competing Fe(III)/Fe(II) reduction has also been observed in a chloride-based Cu-Fe-Au solution, leading to an increased purity of Au product, i.e., the Au/Cu ratio was 3.7 in the presence of Fe, higher than the ratio of 2.9 without Fe [119].

The spontaneous corrosion of the deposited metals in the presence of oxidants is also a typical side reaction: for instance, Cu deposited in a chloride solution can be corroded by dissolved O_2 or by Cu(II) (Fig. 5b) [44], and Zn deposited in an acid solution is corroded in the presence of H^+ (Fig. 5c) [54]. Such corrosion processes increase the energy consumption (lower current efficiency) for noble metal recovery, especially when the dissolution of sacrificial metals is rapid at the beginning of the RR step without participating in replacement. Another side reaction is the H_2 evolution discussed above, which occurs in an acidic solution during the ED step (Fig. 5c). It is noteworthy, however, that corrosion products such as Cu(I) species and evolved H_2 may further act as reductants to recover noble metals, promoting the recovery of the end-product (Fig. 5b and c) [44,54,122].

3.6. Engineering aspects of metal recovery by EDRR

As EDRR is not yet in full use on industrial scale, very few engineering aspects related to EDRR have been published in the open literature. Utilities needed in the process are limited to the use of electricity (needed in the ED step as well as for the inlet solution pump), which dictates the operating expenditure (OPEX) values. Similarly to conventional electrolysis cell equipment, one or several pieces of EDRR equipment can be run for state-of-the-art hydrometallurgical processes using alternative operating strategies (batch process, continuous process, co-current, counter current) in parallel or in series [71]. Also, full (100 %) recovery by such an EDRR process cannot always be the target, and optimization has to be balanced between process time (flowrate) and target recovery, as well as holistic processing at the plant [71]. For instance, in the study of Te recovery from Doré slag PLS (Te: 421 mg L^{-1} and other species at high concentrations, i.e., g L^{-1}), EDRR was found to be competitive with EW when the Te content decreased to <300 mg L^{-1} [45]. The Te content only increased by around 6 wt% on the electrode from 20 min to 96 h (55 wt% after 20 min) by EW. Nevertheless, the capacitive double-layer charging during EDRR that occurs at the beginning of each ED step reduces the energy efficiency. In addition, Te may also dissolve back into the electrolyte during the RR step. Thus, the combined operation of EW (96 h) and EDRR (96 h) in series was introduced to maximize the Te recovery from Doré slag PLS at mg L^{-1} levels (Fig. 6a, >37 wt%). The combined EW + EDRR process could also be beneficial to the overall profitability of a copper factory, as Te is a side product resulting from the treatment of copper anode slime.

To verify the feasibility on industrial scale, a pilot test of EDRR for Au recovery was studied [71]. Four-unit operations, consisting of cupric chloride leaching, filtration, EDRR recovery, and Cu precipitation, were run in semi-continuous mode. A solids concentration of 200 g L^{-1} was maintained in the PLS and the Au concentration in the solution for EDRR was kept above 1 mg L^{-1}. After 150 h of continuous operation (8 h for leaching in each stage, 14 rounds of the leaching-EDRR process), over 80 % of the dissolved Au had been recovered on the cathode (Fig. 6b, Au recovery gradually increases stage by stage), achieving a 68.5 % holistic recovery of Au from ore. The Au content of the final deposit was 58.2 % with an increased Au:Cu ratio from 3.5 × 10^{-5} (PLS) to 1.4 (cathode), i.e., an enrichment factor of 40 000. Compared to conventional cyanide-based technologies, the electro-hydrometallurgical chloride process not

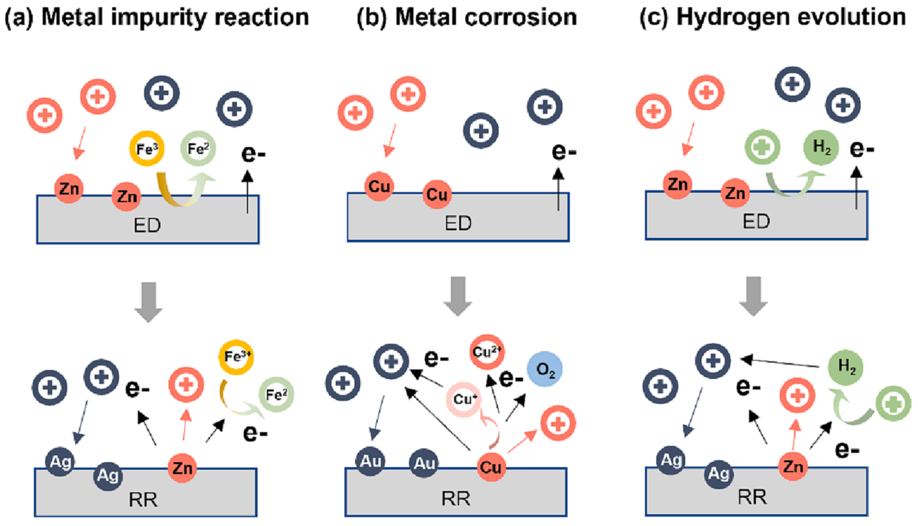

Fig. 5. Typical side reactions in the EDRR process. a) Metal impurity reaction. b) Metal corrosion. c) Hydrogen evolution.

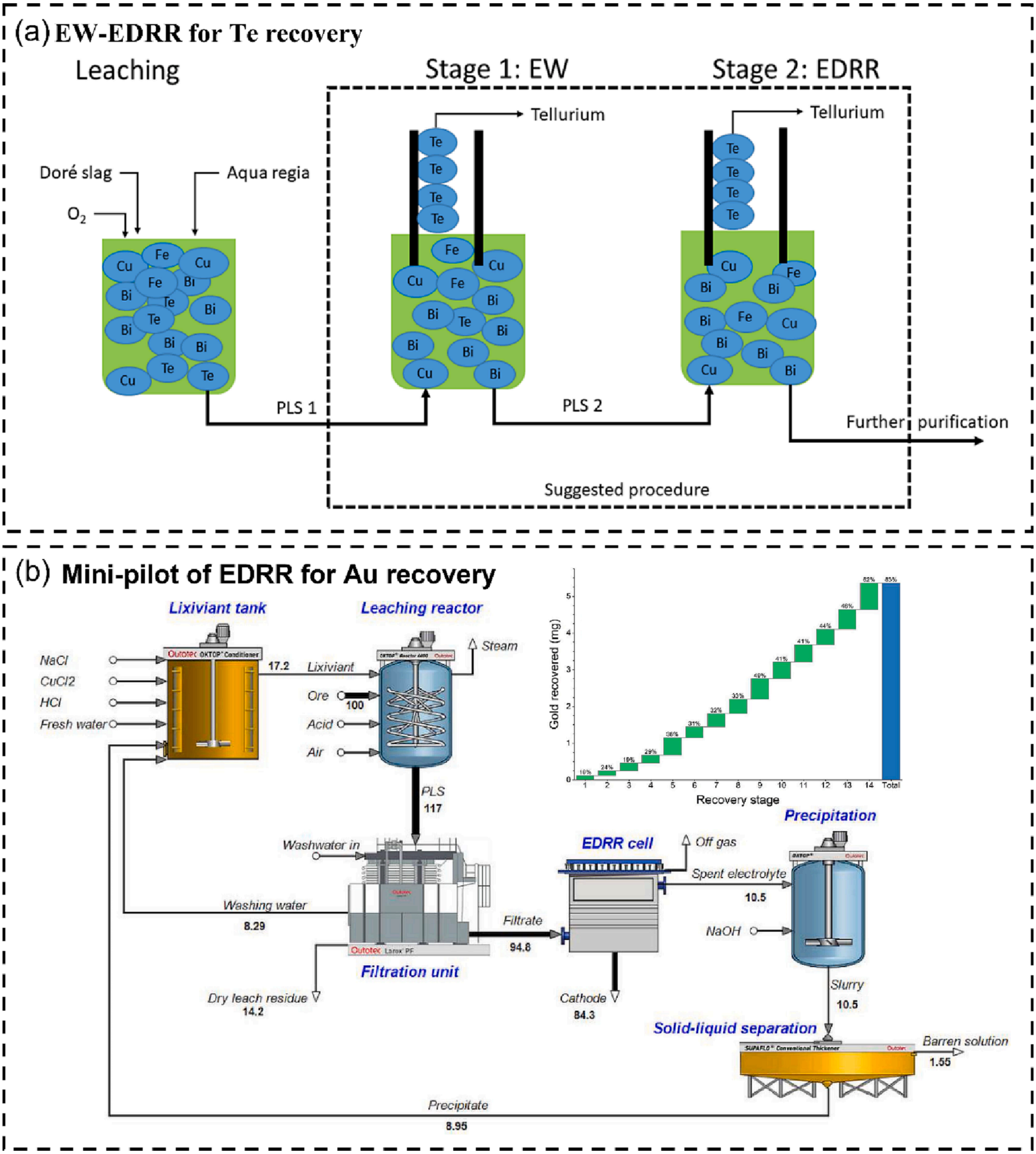

Fig. 6. EDRR conducted in cascade mode. a) Schematic of the proposed EW-EDRR route for Te recovery. Reproduced with permission [45]. Copyright 2020, Springer. b) Schematic of continuous pilot-scale experiment for Au recovery, inset: Au recovered from PLS in each round. Reproduced with permission [71]. Copyright 2022, Elsevier.

only achieves higher Au leaching efficiency (approx. 90 %) directly from the ground ore to solution (cyanidation test: 64 %) but simplifies the unit operations after leaching (purification and concentration by carbon adsorption and elution in cyanide processes) [123]. Moreover, the EDRR cathode is continuously covered by a thin Cu-Au film, leading to less overpotential for the nucleation and growth of Cu. As a result, the energy consumption for EDRR declines with running time (31.4 kWh kg^{-1} in the first stage, 10–15 kWh kg^{-1} in the following rounds), indicating the advantage of EDRR in longer processing time. As energy is only consumed during the ED step, EDRR is beneficial in optimizing the energy consumption in the whole pilot test. The simulated closed-loop operation suggested the potential to recover over 84 % of the Au on the EDRR cathode (Fig. 6b), further indicating the promise of EDRR in sustainable Au extraction [71].

The combined methods involving EDRR offer maximization routes for metal recovery from industrial solutions, not only advancing the sustainable circular economy of metals, but promoting the increase of EDRR to technology readiness levels in the future. However, to develop EDRR as a realistic alternative to conventional techniques to join the holistic industrial plant for metal processing, continuous optimization of performance and comprehensive assessment of the bottlenecks of the industrial scale process are still necessary.

The material selection for EDRR equipment varies, as in any other metallurgical process design. The high acidity and high concentration of oxidative species in complex solutions challenge the selection not only of equipment but also of electrode materials. In laboratory-scale EDRR research, Pt has been the main electrode for Ag [38–40], Au [42,43], and Te [45,46] recovery, although a porous pyrolytic carbon electrode [22] has also served as the cathode for Pt recovery. However, these high value electrode materials are not typically applicable on industrial scale. Considering commercial materials with lower cost, a series of cathode materials such as C-2000 nickel alloy, grade 2 titanium, and 316L and 654SMO stainless steels have been studied for EDRR in cupric chloride solutions [124]. 654SMO steel has been suggested as the most suitable electrode due to its high corrosion resistance (corrosion rate of 0.02 mm/year) and cost effectiveness. In the open literature, there are no publications yet about anode material selection for EDRR. In industrial electrowinning, state-of-the-art anode materials are based on Pb or mixed metal oxides [125,126], whereas in EDRR operation, Pb could result in spontaneous cementation and potential losses of target metals. For collection, the deposited metals can be mechanically stripped away, similarly to conventional EW or ER. Chemical stripping (leaching), typically used for precious metals production (e.g., in concentrated HCl solution) or electrochemical stripping can also be used.

4. EDRR for controllable metal deposits and their functional properties

Sourcing directly from industrial process streams, EDRR leads to advances not only in metal recovery, but also in simple fabrication of diverse metal deposits, including Pt/Ni [52], Ag/Cu [53], Ag/Zn [54,55], Cu/Zn [56], and Cu/Zn/Ag [57] (Table 4). The morphology, structure, composition, and even the functional properties of the metal deposits obtained by EDRR are highly process dependent and thus controllable. EDRR is also compatible with various conductive substrates, enabling selective functionalization of both metal deposits and diverse substrates.

Table 4
EDRR for metal depositions and functional materials.

Metals	Precursor solution	Media	Investigated parameters	Structure and functional properties of the metal depositions	Ref. No.
Pt/Ni (2018)	Synthetic Ni process solution: Ni: 60 g/L H_2SO_4: 10 g/L Pt: 100 mg L^{-1}	sulfate	i(cathodic) = 100 mA/cm^2 for 10 ms, i (anodic) = 20 mA/cm^2 for 10 ms, total number of pulses: 74 (37 cathodic-anodic pulse pairs) ***t*₂**: 10, 30, 60, 120, 240 s ***n***: 10–30	Jagged nanoparticles **photocatalyst**	[52]
Ag/Cu (2019)	Synthetic Cu process solution: H_2SO_4: 120 g/L Cu: 40 g/L Ag: 1–10 mg L^{-1}	sulfate	E_1: −0.5, −0.1 V vs Ag/AgCl t_1: 50, 500 ms t_2: 2, 50, 100 150, 300, 600 s n: 20	Nanoparticles	[53]
Ag/Zn (2021)	Synthetic Zn process solution: Zn: 65 g/L H_2SO_4: 10 g/L Ag: 0.5–50 mg L^{-1}	sulfate	E_1: −1.65, −1.60, −1.55 V vs SCE t_1: 0.5 s t_2: 0.5, 5, 10, 20, 30, 50, 100, 200 s n: 30	Nanoparticles	[54]
Ag/Zn (2022)	Synthetic Zn process solution: Zn: 65 g/L H_2SO_4: 10 g/L Ag: 20 mg L^{-1}	sulfate	E_1: −1.65, −1.55 V vs Hg/Hg_2SO_4 t_1: 0.5, 1 s t_2: 10, 20 s n: 400	Dendrites and nanoparticles **SPR**	[55]
Cu/Zn (2022)	Synthetic Zn process solution: Zn: 65 g/L H_2SO_4: 10 g/L Ag: 200 mg L^{-1}	sulfate	E_1: −1.55 V vs Hg/Hg_2SO_4 t_1: 0.3, 0.5 s t_2: 5, 10, 20, 40 s n: 200	Spiky nanoparticles and coatings **Corrosion resistance**	[56]
Cu/Zn/Ag (2022)	Synthetic Zn process solution: Zn: 65 g/L Cu: 200 mg L^{-1} H_2SO_4: 10 g/L Ag: 2 mg L^{-1}	sulfate	E_1: −1.55 V vs Hg/Hg_2SO_4 t_1: 0.3, 0.5 s t_2: 5, 10, 20 s n: 400	Nanoparticles and coatings **SPR and corrosion resistance**	[57]

4.1. *Morphology of EDRR deposition*

The metals recovered by EDRR can be porous deposits, micrometer-sized clusters, or nanoparticles, which are either individually distributed or form a continuous film. The metal deposition of EDRR is usually less compact compared to EW deposition (e.g., recovered Ag, Au, and Te), which is a result of base metal dissolution (Fig. 7a and b) [38,42,45]. As the RR step of EDRR takes place only with a small amount of sacrificial metal in each cycle, EDRR-based deposition is more homogeneous with less agglomeration compared to metals recovered by cementation (Fig. 7c and d, Ag particles recovered by EDRR were smaller) [53]. Also, H_2 evolution causes uneven distribution of the local current, resulting in non-uniform morphologies (when Zn or Ni is used as the sacrificial metal, Fig. 7e) [22,38,40]. Moreover, the metal deposition obtained by EDRR is not always evenly distributed over the electrode: the current density at the edge of the electrodes is usually higher than in the center area, resulting in an increased deposition rate and bigger deposits [41]. In a flow cell with an alternating flux of electrolyte, bigger deposits of noble metal were observed on the inlet side (Fig. 7f), which was exposed to the fresh injected solution first. Non-homogenous distribution needs further investigation to build material design guidelines, especially for applications that require accurate metal nanoparticle distribution.

4.2. *Controllable metal deposition by EDRR*

4.2.1. *Influence of EDRR parameters*

The elemental composition of the metal deposits can be tuned by means of EDRR parameters. A more negative E_1 or longer t_1 typically results in a higher concentration of sacrificial metals in the final surface. Taking Ag-based deposition as an example, the Zn content in Zn/Ag was

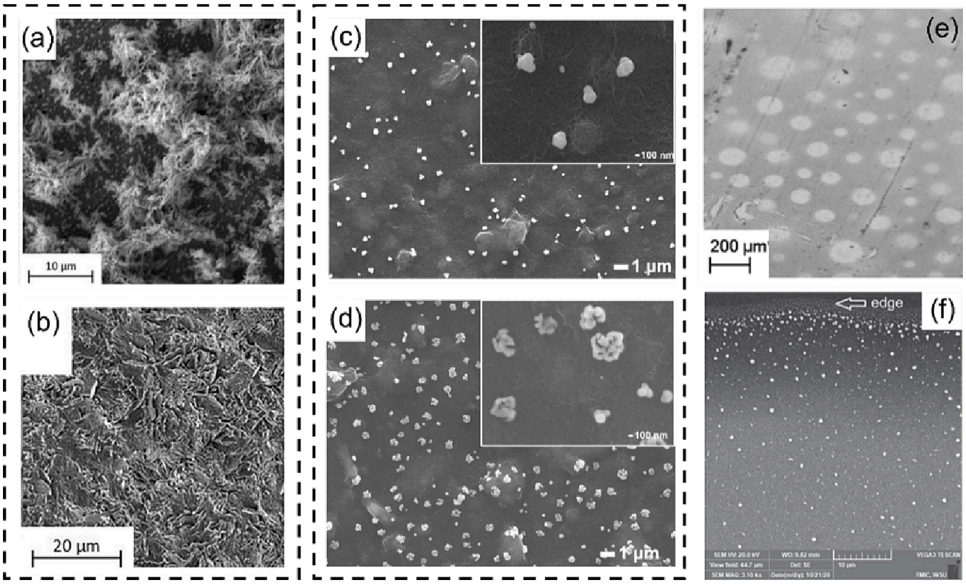

Fig. 7. Scanning electron microscope (SEM) images of metals deposited on the electrodes by EDRR. a) Te deposition by EDRR. b) Te deposition by EW. (a-b) Reproduced with permission [45]. Copyright 2020, Elsevier. c) Ag/Cu particles obtained by EDRR. d) Ag/Cu particles obtained by cementation. (c-d) Reproduced with permission [53]. Copyright 2019, Elsevier. e) Effect of H_2 evolution on EDRR deposition (round, lighter color spots). Reproduced with permission [38]. Copyright 2018, American Chemical Society. f) Distribution of Ag particles on the electrode after EDRR. Reproduced with permission [41]. Copyright 2021, Elsevier.

72 at% and 27 at% when utilizing an E_1 of −1.65 V and −1.55 V, respectively [55]. It is understandable that the designated E_2 or t_2 of RR reactions has a significant influence on the composition of the metal deposit, as the interruption of RR leads to insufficient replacement of sacrificial metals. A longer t_2 or more positive E_2 enhances the content of noble metals in the final deposits and a longer t_2 also facilitates the selective dissolution of sacrificial metals (e.g., by Fe impurity), further leading to the higher purity of noble metals on the electrode. When

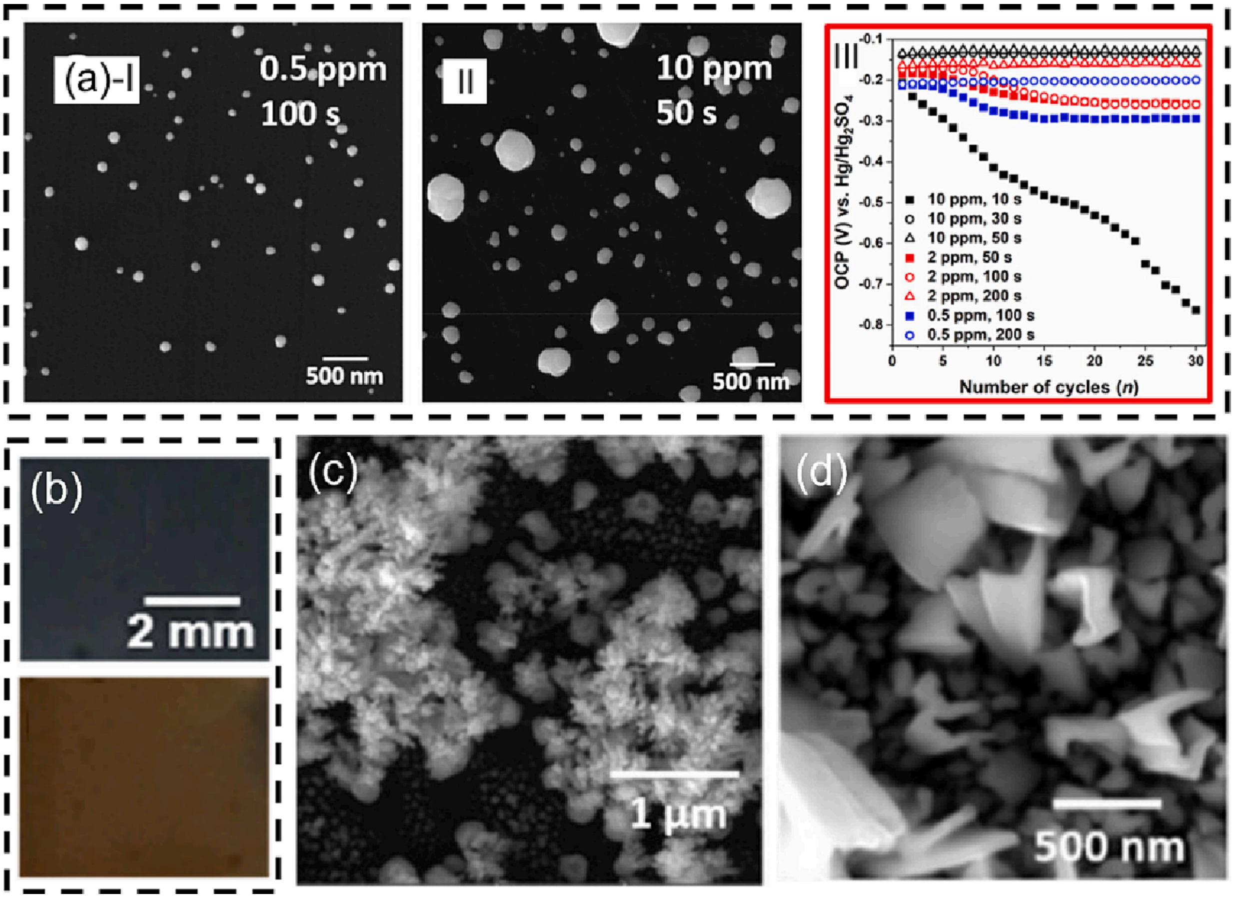

Fig. 8. Influence of mass transfer limitation on EDRR deposition. a) SEM and OCP values of Ag/Zn nanoparticles obtained from solutions with different Ag concentrations and varying t_2. Reproduced with permission [54]. Copyright 2021, American Chemical Society. b) Photos of Cu/Zn alloys, upper: no stirring with lower Cu content, lower: under stirring with higher Cu content. Reproduced with permission [56]. Copyright 2022, American Chemical Society. c) SEM of dendritic Ag/Zn nanoparticles. Reproduced with permission [55]. Copyright 2022, American Chemical Society. d) SEM of spiky Cu/Zn nanoparticles. Reproduced with permission [56]. Copyright 2022, American Chemical Society.

changing $\boldsymbol{t_2}$ from 0 to 50 s, the Ag content in Ag/Zn increased from 0 to 31 at% [54], and the Cu content in the Cu/Zn deposits changed from 27 at% to 77 at% when the applied $\boldsymbol{t_2}$ was 10–40 s [56].

The size of the deposits tended to increase with $\boldsymbol{t_1}$ [53,55] or $\boldsymbol{t_2}$ [52–54], as a longer electrodeposition time allows the formed nuclei to grow [127]. For instance, the Cu/Ag particles were 637 ± 144 nm and 837 ± 323 nm when $\boldsymbol{t_1}$ was 50 ms and 500 ms, respectively [53], and the particle size of Ag/Zn was 39 ± 16 nm and 186 ± 100 nm when $\boldsymbol{t_2}$ was 5 and 50 s, respectively [54]. It should be noted that the particle distribution was less uniform especially for larger particles, due to Ostwald ripening; a similar phenomenon was also observed in Ag/Cu, Ag/Zn, and Pt/Ni obtained through EDRR [52–54]. The metal deposits grow with EDRR cycles as well [52,54,56], and the continuously growing deposits tend to coalesce with each other and form a complete layer [56].

4.2.2. *Influence of mass transfer*

A low noble metal concentration significantly limits mass transfer during the RR reaction [128,129]. Either the noble metal content or the size of the deposited nanoparticle increases if a higher initial concentration of noble metals is present in the solution (Fig. 8a) [54]. When the system is equipped with agitation, the RR reaction kinetics also changed with enhanced mass transfer [52–54]. To take two examples: the Cu content in Cu/Zn increased from 15 % to 67 % under stirring (Fig. 8b, the color of the alloy varies with the composition) [56]; the average sizes of Ag/Zn deposits were 39 ± 6 nm and 114 ± 52 nm with and without stirring, respectively [54]. However, the enhanced flow rate of the electrolyte during agitation may remove the metal deposit unless the adhesion between the metal deposits and the electrode surface is strong enough, implying that the optimization of solution movement is required [54].

Mass transfer can also be controlled using EDRR parameters to tailor metal deposits with different structures, such as dendritic Ag/Zn (Fig. 8c) and spiky Cu/Zn (Fig. 8d) [55,56]. Mass transfer limitation can be formed in either the ED or RR step. For instance, a higher overpotential and longer $\boldsymbol{t_1}$ in the ED step results in more deposition of the sacrificial metal. At the same time, if a shorter $\boldsymbol{t_2}$ is applied in the RR step, there is insufficient migration of the metal species from the solution to the electrode, causing mass transfer limitation. Specifically, to obtain dendritic Ag/Zn, the gradient of Zn concentration formed first near the electrode due to the mass transfer limitation, then the growth of dendritic Ag/Zn started from the larger nanoparticles and enlarged into branch-like features gradually [55]. The spiky Cu/Zn alloy [56] was mainly the result of the screw dislocation of Zn atoms in the ED step due to the limited diffusion of Zn^{+} and hindered electron transfer. The H_2 produced and the lower Cu concentration as well as the shorter $\boldsymbol{t_2}$ further facilitated the formation of spiky structures [130–133]. Extended EDRR cycles are favorable to maintain such mass transfer limitation.

4.3. *Functional properties and applications of EDRR deposition*

EDRR deposition has demonstrated its potential usefulness for functional materials. For example, the Pt/Ni deposited on a TiO_2 nanotube exhibited strong activity for photocatalytic H_2 evolution, which is important in contributing to clean energy and addressing the severe climate challenges in our society [52]. The higher the ratio of Pt/Ni, the better the photocatalytic activity (Fig. 9a), and the composition of Pt/Ni nanoparticles can be controlled by the EDRR parameters [52]. Therefore, EDRR offers a sustainable circular economy platform to prepare photocatalysts, indicating the possibility of hydrometallurgical streams as a substitute for raw material sources for industrial catalyst production.

Moreover, other metal deposits created by EDRR showcased further properties, such as surface plasmon resonance (SPR) and corrosion-resistance. SPR is a significant technique used in medical diagnostics, biological detection, environmental monitoring, food safety [134]. EDRR enabled the production of SPR surfaces also through the dealloying route, based on the distinct dissolution potentials of the alloyed metals (Fig. 9b and c) [55–57]. The structure, chemical composition, and crystalline phases of EDRR-based metal deposits play important roles in their corresponding functionalities. Specifically, dealloyed Ag-rich dendrites showed dual-peak SPR behavior (S1 and S2-S6 after dealloying in Fig. 9b), whereas a single peak was achieved both in Ag/Zn and dealloyed Ag-rich spherical particles (S2 after dealloying in Fig. 9b) [55]. A Zn-rich Cu/Zn coating (containing $CuZn_5$ and Cu_5Zn_8 phases), on the other hand, exhibited lower corrosion resistance (with higher J_{corr} in Fig. 9c) than a Cu-rich Cu/Zn coating (containing $Cu_{0.75}Zn_{0.25}$ and $Cu_{0.85}Zn_{0.15}$ phases) [56]. It is also noteworthy that EDRR allows the production of metal deposits with selective functionalities from the same multi-metal solutions: in a Zn process solution (with Zn, Cu, and Ag), the uniform Cu/Zn/Ag coating obtained was corrosion-resistant if Zn served as the sacrificial element; however, when using Cu as the sacrificial metal, the Cu/Ag nanoparticles formed exhibited SPR properties [57]. These findings are promising, given the early stage of EDRR research in multi-functional materials.

4.4. *Substrates for EDRR metal deposition*

Any conductive materials which are stable (i.e., no corrosion) in an EDRR solution can theoretically be substrates for deposition, such as glassy carbon utilized to obtain Ag/Zn, Cu/Zn, and Cu/Zn/Ag deposits

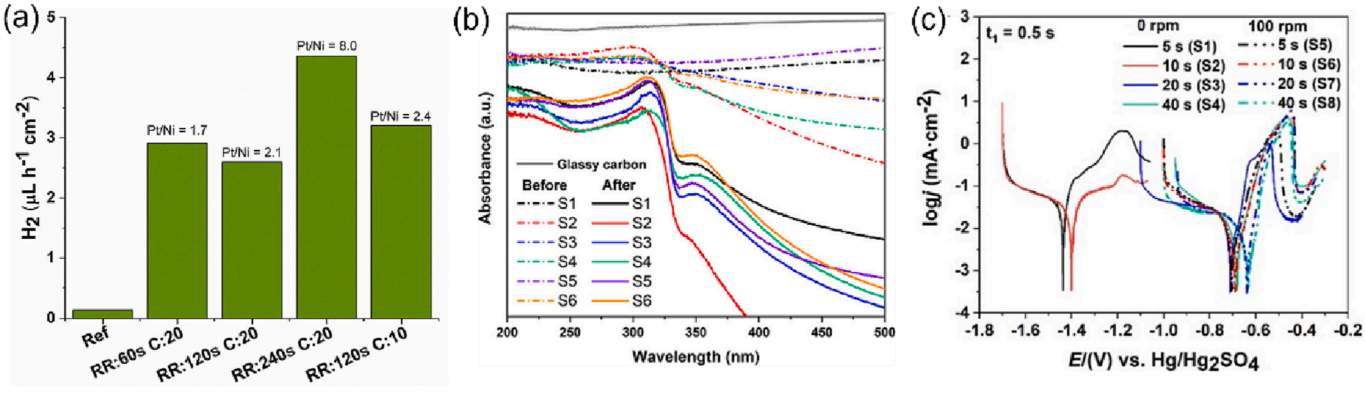

Fig. 9. Functional application and properties of EDRR deposition. a) H_2 evolution performances of $Pt/Ni/TiO_2$ photocatalysts. Reproduced with permission [52]. Copyright 2018, Elsevier. b) UV − vis spectra of as-prepared EDRR samples (with varying E_1, t_1, and t_2) before and after dealloying. Reproduced with permission [55]. Copyright 2022, American Chemical Society. c) Corrosion resistant performances of Cu/Zn samples obtained by EDRR with different t_2, Zn-rich Cu/Zn: E_{corr} of −1.39 V- −1.44 V vs Hg/Hg_2SO_4 and J_{corr} of 10.9–25.7 μA/cm^2, Cu-rich Cu/Zn: E_{corr} of −0.67 V vs Hg/Hg_2SO_4 and J_{corr} of 3.9 μA/cm^2. Reproduced with permission [56]. Copyright 2022, American Chemical Society.

[54–57]. The selection of substrates should also consider the target applications. Based on the photocatalytic activity of TiO_2, both flat TiO_2 and TiO_2 nanotube have served as substrates in EDRR to create Pt/Ni catalysts for H_2 evolution [52]. Thanks to their high surface area and electrical conductivity, carbon nanotube films have been used as metal enrichment substrates to support Cu/Ag nanoparticles [53], with potential applications in sensors, catalysts, and antibacterial surfaces. To further implement EDRR in functional materials, the introduction of diverse patterned 2D and 3D substrates can improve the performance of the current applications and help to reveal totally new uses.

5. Conclusions and outlook

In summary, the EDRR method is beneficial both for metal recovery and creation of functional metal products directly from lower grade complex solutions, satisfying the principles of minimal incorporation of additional chemicals, electrification of metallurgy, and circular economy of materials. Compared to traditional hydrometallurgical processes, EDRR is more efficient at recovering precious metals at the $\mu g\ L^{-1}$ or $mg\ L^{-1}$ level from industrial process or waste solutions. Thus, EDRR can be a competitive and realistic option for recovery of noble metals from impure lower-grade solution. With technologically and economically feasible set-up, EDRR can have a substantial impact on industrial metal recovery and production. Regarding the fabrication of metal materials, EDRR enables the control of the morphology, structure, elemental composition, and functional properties of the metal deposits. However, EDRR is still under development, as energy efficiency needs optimization, the sustainability and material design based on EDRR also require further elucidation (Fig. 10).

5.1. Development of EDRR with optimized energy consumption

The energy consumption of EDRR is crucial when assessing economic and environmental perspectives. The energy consumption is determined by various factors within electrochemical processes, such as the applied potential and current efficiency. The applied potential is not only related to the required overpotentials at the cathode, but also the potential to overcome the resistance of the electrolyte and electrical contacts. The current efficiency is affected by H_2 evolution, deposition/replacement of impurities, oxidation/reduction of multi-valence species, and electrochemical dissolution. The charging of the capacitive double layer at the beginning of each ED cycle also reduces the overall energy efficiency [122,135]. In addition, the longer the EDRR process, the more electrical energy consumed. Better understanding of the limiting factors is beneficial for further optimization of the EDRR parameters toward energy-efficient operation.

Moreover, the RR reaction can be in the form of a solid–liquid reaction (deposition on the electrode surface), gas–liquid reaction (gas evolution), or even liquid–liquid reaction. One proof of a liquid–liquid reaction is the reduction of dissolved Au by the Cu(I) in solution [44]. Such a phenomenon triggers further speculation, i.e., a lower oxidation state of multivalent metal species (less noble) may be enough to recover noble metals in solution. From this point of view, the excessive charge applied to reduce the sacrificial metal species to its elemental state (i.e., zero valence, solid) seems to be "wasted". If the oxidation states or the partial reduction of the sacrificial metal species (e.g., Cu(II) → Cu(I), Fe (III) → Fe(II)) in the solution can be controlled well, the energy consumption of the overall recovery process will be reduced. An end-product of higher purity will also be achieved, as no sacrificial metal appears on the surface in such a process.

5.2. Development of EDRR with improved circular sustainability

With increased demand for recycling electronic waste, catalysts, solar cells, batteries, bottom ash, EDRR is attractive in terms of numerous potential metallurgical solutions. Further research to reveal the influence of different impurity species on recovery efficiency (e.g., purity of end-product and selectivity) is of great importance. The recovery and/or impurity management by EDRR would be an efficient option to prevent material losses and further increase the market value of the metal production. Moreover, if the trace metals ($\mu g\ L^{-1}$ – $mg\ L^{-1}$) present in recyclable wastes are fully utilized by EDRR, the corresponding environmental burden of virgin production (e.g., the losses of metal to landfill) can be alleviated. It is necessary to evaluate the holistic performance, e.g., by simulation-based life cycle analysis to confirm the sustainability of any new process [136–139]. To consider the principles of the circular economy further, the equipment construction materials (i.e., electrodes and electrolysis cell) and their environmental footprint should be investigated. The electrode materials can also be sourced from diverse waste materials. For instance, carbonized food industry waste and polysaccharides are promising building blocks for constructing highly controlled porous 3D electrodes for EDRR.

5.3. Development of EDRR for the design of functional materials

EDRR has already been employed to create Pt photocatalysts for H_2 generation from a simulated hydrometallurgical solution [52], indicating that EDRR can support material sufficiency in the hydrogen economy and thus contribute to renewable energy. The suitability of diverse functional materials by EDRR from various waste materials for large-scale production and their quality in commercial applications will be continuously developed and improved. More applications based on single metal, bi- or multi-metals, such as catalysts, plasmonic sensors, energy conversion and storage, as well as antibacterial/antiviral applications, can be explored with the materials created by EDRR. Numerous functional 3D networks are promising as electrodes for EDRR to achieve modification of the inner surface, suggesting the potential of EDRR in applications based on porous or crosslinked structures. For instance, in photocatalytic applications, the collection of incoming light needs to be optimized, which could be achieved upon different porous networks

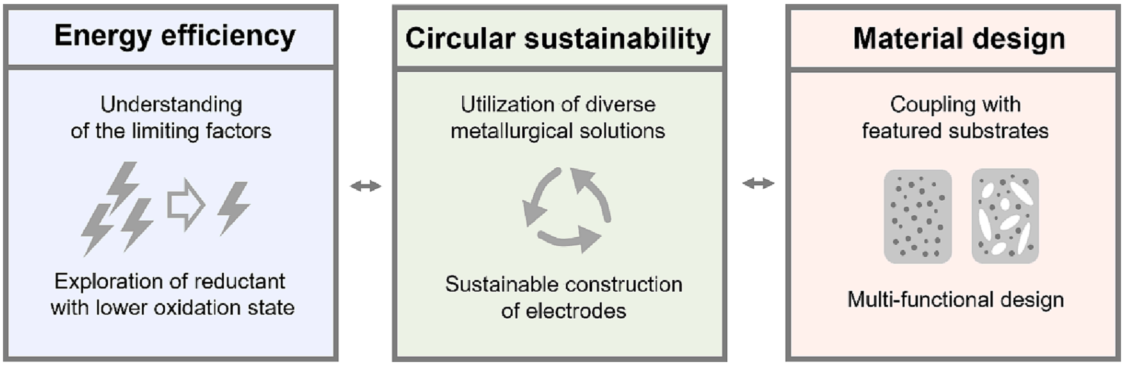

Fig. 10. Future prospects of EDRR.

with a surface modified by EDRR. Through precise control of the materials with their morphology, distribution, composition, and crystalline structure, the design of stimuli responsive materials can also be coupled with EDRR to realize more complicated functions, such as light or thermally trigged antibacterial, sensing, or catalytic behaviors. Thus, various potential applications based on EDRR methodology are yet to be explored.

Overall, EDRR offers an efficient approach for refining valuable metals and even manufacturing functional materials directly, exploiting the currently underutilized hydrometallurgical process solutions to advantage. EDRR routes tapping into enhanced energy efficiency, improved circular economics, and wider application fields, are expected to contribute to existing and future materials in an environmentally sustainable way.

Declaration of Competing Interest

The authors declare the following financial interests/personal relationships which may be considered as potential competing interests: Mari Lundstrom, Kirsi Yliniemi are the inventors of patent #A method for recovering Pt and Ag from sulphuric acid base metal solutions (PCT/FI2018/050484) issued to Elmery Oy. Mari Lundstrom, Kirsi Yliniemi are the inventors of patent #A method of recovering copper from a dilute metal containing solution (FI127471 (granted), CL2019-1710, PE001279-2019/DIN, US16/471586, ZA2019/03951, P0020190 61081) issued to Elmery Oy.

Data availability

Data will be made available on request.

Acknowledgments

This review was supported by the Academy of Finland project EARMetal (LC, KY, ML: 339979 and LC, KY, JV: 342080). The RawMatTERS Finland Infrastructure (RAMI) funded by the Academy of Finland and based at Aalto University is also acknowledged.

References

[1] S.M. Jowitt, G.M. Mudd, J.F.H. Thompson, Future availability of non-renewable metal resources and the influence of environmental, social, and governance conflicts on metal production, Commun. Earth Environ. 1 (2020) 13, https://doi.org/10.1038/s43247-020-0011-0.

[2] Q. Dehaine, S.P. Michaux, J. Pokki, M. Kivinen, A.R. Butcher, Battery minerals from Finland: Improving the supply chain for the EU battery industry using a geometallurgical approach, EurGeol. 49 (2020) 5–11, https://doi.org/10.5281/zenodo.3938855.

[3] H.U. Sverdrup, A.H. Olafsdottir, K.V. Ragnarsdottir, On the long-term sustainability of copper, zinc and lead supply, using a system dynamics model, Resour. Conserv. Recycl.: X 4 (2019), 100007, https://doi.org/10.1016/j.rcrx.2019.100007.

[4] R.B. Gordon, M. Bertram, T.E. Graedel, Metal stocks and sustainability, PNAS 103 (2006) 1209–1214, https://doi.org/10.1073/pnas.0509498103.

[5] H. Sverdrup, D. Koca, K.V. Ragnarsdottir, Investigating the sustainability of the global silver supply, reserves, stocks in society and market price using different approaches, Resour. Conserv. Recycl. 83 (2014) 121–140, https://doi.org/10.1016/j.resconrec.2013.12.008.

[6] H.U. Sverdrup, K.V. Ragnarsdottir, D. Koca, On modelling the global copper mining rates, market supply, copper price and the end of copper reserves, Resour. Conserv. Recycl. 87 (2014) 158–174, https://doi.org/10.1016/j.resconrec.2014.03.007.

[7] S. Northey, S. Mohr, G.M. Mudd, Z. Weng, D. Giurco, Modelling future copper ore grade decline based on a detailed assessment of copper resources and mining, Resour. Conserv. Recycl. 83 (2014) 190–201, https://doi.org/10.1016/j.resconrec.2013.10.005.

[8] G.M. Mudd, S.M. Jowitt, T.T. Werner, The world's by-product and critical metal resources part I: Uncertainties, current reporting practices, implications and grounds for optimism, Ore Geol. Rev. 86 (2017) 924–938, https://doi.org/10.1016/j.oregeorev.2016.05.001.

[9] T.T. Werner, G.M. Mudd, S.M. Jowitt, The world's by-product and critical metal resources part III: A global assessment of indium, Ore Geol. Rev. 86 (2017) 939–956, https://doi.org/10.1016/j.oregeorev.2017.01.015.

[10] T.T. Werner, G.M. Mudd, S.M. Jowitt, The world's by-product and critical metal resources part II: A method for quantifying the resources of rarely reported metals, Ore Geol. Rev. 80 (2017) 658–675, https://doi.org/10.1016/j.oregeorev.2016.08.008.

[11] C.-M. Backman, Global Supply and Demand of Metals in the Future, J. Toxic. Environ. Health A 71 (2008) 1244–1253, https://doi.org/10.1080/15287390802209582.

[12] R.A. Kerr, The Coming Copper Peak, Science 343 (2014) 722–724, https://doi.org/10.1126/science.343.6172.722.

[13] S. Michaux, Assessment of the Extra Capacity Required of Alternative Energy Electrical Power Systems to Completely Replace Fossil Fuels, 2021. https://doi.org/10.13140/RG.2.2.34895.00160.

[14] G. Reverdiau, A. le Duigou, T. Alleau, T. Aribart, C. Dugast, T. Priem, Will there be enough platinum for a large deployment of fuel cell electric vehicles? Int J Hydrog Energy 46 (2021) 39195–39207, https://doi.org/10.1016/j.ijhydene.2021.09.149.

[15] S.R. Rao Hydrometallurgical Processes S.R. Rao Resource Recovery and Recycling from Metallurgical Wastes Vol. 7 2006 Elsevier Amsterdam 71 108 10.1016/S0713-2743(06)80089-9 Waste Management Series.

[16] T.K. Rose, The Metallurgy of Gold, second ed., C. Griffin, London, 1894.

[17] H. Davy, I. The Bakerian Lecture, on some chemical agencies of electricity, Philos. Trans. R. Soc. Lond. 97 (1807) 1–56, https://doi.org/10.1098/rstl.1807.0001.

[18] S. Jafari, M. Kiviluoma, T. Kalliomäki, E. Klindtworth, A.T. Aji, J. Aromaa, B. P. Wilson, M. Lundström, Effect of typical impurities for the formation of floating slimes in copper electrorefining, Int. J. Miner. Process. 168 (2017) 109–115, https://doi.org/10.1016/j.minpro.2017.09.016.

[19] F. Vegliò, R. Quaresima, P. Fornari, S. Ubaldini, Recovery of valuable metals from electronic and galvanic industrial wastes by leaching and electrowinning, Waste Manag. 23 (2003) 245–252, https://doi.org/10.1016/S0956-053X(02)00157-5.

[20] C. Anderson G, Optimization of Industrial Copper Electro Winning Solutions J Adv Chem Eng. 7 2017 1000156 10.4172/2090-4568.1000156.

[21] Y. Khouraibchia, M.S. Moats, Evaluation of the Effect of Copper Electrowinning Parameters on Current Efficiency and Energy Consumption Using Surface Response Methodology, ECS Trans. 28 (2010) 295–306, https://doi.org/10.1149/1.3367922.

[22] P. Halli, J.J. Heikkinen, H. Elomaa, B.P. Wilson, V. Jokinen, K. Yliniemi, S. Franssila, M. Lundström, Platinum Recovery from Industrial Process Solutions by Electrodeposition-Redox Replacement, ACS Sustain. Chem. Eng. 6 (2018) 14631–14640, https://doi.org/10.1021/acssuschemeng.8b03224.

[23] F.K. Crundwell M.S. Moats V. Ramachandran T.G. Robinson W.G. Davenport Electrowinning of Nickel from Purified Nickel Solutions F.K. Crundwell M.S. Moats V. Ramachandran T.G. Robinson W.G. Davenport Extractive Metallurgy of Nickel, Cobalt and Platinum Group Metals 2011 Elsevier, Oxford 327 345 10.1016/B978-0-08-096809-4.10026-7.

[24] D. Robinson, F.C. Walsh, Silver Removal from an X-Ray Fixer Solution by means of a Potentiostatically-Controlled Rotating Cylinder Electrode, J Photogr Sci 42 (1994) 182–192, https://doi.org/10.1080/00223638.1994.11738599.

[25] Y. Su, Q. Li, Y. Wang, H. Wang, J. Huang, X. Yang, Electrochemical reclamation of silver from silver-plating wastewater using static cylinder electrodes and a pulsed electric field, J. Hazard. Mater. 170 (2009) 1164–1172, https://doi.org/10.1016/j.jhazmat.2009.05.096.

[26] R. Winand, Electrocrystallization – theory and applications, Hydrometall. 29 (1992) 567–598, https://doi.org/10.1016/0304-386X(92)90033-V.

[27] U.S. Geological Survey Mineral commodity summaries 2022 2022 Reston 10.3133/mcs2022.

[28] M. Maja, P. Spinelli, Detection of Metallic Impurities in Acid Zinc Plating Baths, J. Electrochem. Soc. 118 (1971) 1538–1540, https://doi.org/10.1149/1.2408373.

[29] P. Kangas P. Koukkari B. Wilson M. Lundström J. Rastas P. Saikkonen J. Leppinen V. Hintikka Hydrometallurgical Processing of Jarosite to Value-Added Products Conference in Minerals Engineering 2017 Luleå.

[30] T. Kalliomäki, A. Aji, J. Aromaa, M. Lundström, Settling properties of copper electrorefining anode slimes, in: Proceedings of the 58th Conference of Metallurgists Hosting Copper, Vancouver, 2019.

[31] M. Lundström, K. Yliniemi, A method of recovering gold from a gold-bearing concentrated copper chloride solution, WO/2017/216417. https://patents.google.com/patent/WO2017216417A1.

[32] M. Lundström, K. Yliniemi, Method of recovering copper from a dilute metal containing solution, WO/2018/115580.

[33] M. Lundström, K. Yliniemi, P. Halli, S. Franssila, V. Jokinen, J. Heikkinen, A method of recovering Pt or Ag or Pt and Ag from sulfate based metal solutions, WO/2018/234637. https://patents.google.com/patent/WO2018234637A1/en (accessed November 24, 2022).

[34] N.P. Brandon, M.N. Mahmood, P.W. Page, C.A. Roberts, The direct electrowinning of gold from dilute cyanide leach liquors, Hydrometall. 18 (1987) 305–319, https://doi.org/10.1016/0304-386X(87)90072-7.

[35] A.C. Kasper, H.M. Veit, M. García-Gabaldón, V.P. Herranz, Electrochemical study of gold recovery from ammoniacal thiosulfate, simulating the PCBs leaching of mobile phones, Electrochim. Acta 259 (2018) 500–509, https://doi.org/10.1016/j.electacta.2017.10.161.

[36] M. Bae, H. Kim, S. Kim, H. Lee, Electrowinning of gold from a dilute solution using hydrocyclone-type cell, Geosystem Eng. (2022), https://doi.org/10.1080/12269328.2022.2142855.

[37] J. Hong, Z. Xu, D. Li, X. Guo, D. Yu, Q. Tian, A pilot study: Efficient electrowinning of tellurium from alkaline solution by cyclone electrowinning

technology, Hydrometall. 196 (2020), 105429, https://doi.org/10.1016/j.hydromet.2020.105429.
[38] P. Halli, H. Elomaa, B.P. Wilson, K. Yliniemi, M. Lundström, Improved Metal Circular Economy-Selective Recovery of Minor Ag Concentrations from Zn Process Solutions, ACS Sustain. Chem. Eng. 5 (2017) 10996–11004, https://doi.org/10.1021/acssuschemeng.7b02904.
[39] H. Elomaa, P. Halli, T. Sirviö, K. Yliniemi, M. Lundström, A future application of pulse plating – silver recovery from hydrometallurgical bottom ash leachant, Trans. Inst. Met. Finish. 96 (2018) 253–257, https://doi.org/10.1080/00202967.2018.1507320.
[40] Z. Wang, P. Halli, P. Hannula, F. Liu, B.P. Wilson, K. Yliniemi, M. Lundström, Recovery of Silver from Dilute Effluents via Electrodeposition and Redox Replacement, J. Electrochem. Soc. 166 (2019) E266–E274, https://doi.org/10.1149/2.0031910jes.
[41] D.E. Molina, N. Wall, H. Beyenal, C.F. Ivory, Flow Injection Electrochemical Quartz Crystal Microbalance with ICP-OES Detection: Recovery of Silver by Electrodeposition with Redox Replacement in a Flow Cell, J. Electrochem. Soc. 168 (5) (2021) 056518.
[42] I. Korolev, P. Altınkaya, P. Halli, P.-M. Hannula, K. Yliniemi, M. Lundström, Electrochemical recovery of minor concentrations of gold from cyanide-free cupric chloride leaching solutions, J. Clean. Prod. 186 (2018) 840–850, https://doi.org/10.1016/j.jclepro.2018.03.177.
[43] I. Korolev, E. Kolehmainen, M. Haapalainen, K. Yliniemi, M. Lundström, Gold Recovery from Chloride Leaching Solutions by Electrodeposition-Redox Replacement Method, in: U. Waschki (Ed.), Proceedings of the 10th European Metallurgical Conference, Volume 2, GDMB Verlag GmbH, Dusseldorf, 2019: pp. 623–630.
[44] I. Korolev, S. Spathariotis, K. Yliniemi, B.P. Wilson, A.P. Abbott, M. Lundström, Mechanism of selective gold extraction from multi-metal chloride solutions by electrodeposition-redox replacement, Green Chem. 22 (2020) 3615–3625, https://doi.org/10.1039/D0GC00985G.
[45] P. Halli, B.P. Wilson, T. Hailemariam, P. Latostenmaa, K. Yliniemi, M. Lundström, Electrochemical recovery of tellurium from metallurgical industrial waste, J. Appl. Electrochem. 50 (2020) 1–14, https://doi.org/10.1007/S10800-019-01363-6/TABLES/6.
[46] P. Halli, M. Rinne, B.P. Wilson, K. Yliniemi, M. Lundström, Environmental Aspects of the Electrochemical Recovery of Tellurium by Electrochemical Deposition-Redox Replacement (EDRR), in: G. Azimi, T. Ouchi, K. Forsberg, H. Kim, S. Alam, A. Alafara Baba, N.R. Neelameggham (Eds.), Rare Metal Technology 2021, The Minerals, Metals & Materials Series, Springer, Cham, 2021: pp. 57–63. https://doi.org/10.1007/978-3-030-65489-4_7.
[47] K. Yliniemi, D. Wragg, B.P. Wilson, H.N. McMurray, D.A. Worsley, P. Schmuki, K. Kontturi, Formation of Pt/Pb nanoparticles by electrodeposition and redox replacement cycles on fluorine doped tin oxide glass, Electrochim. Acta 88 (2013) 278–286, https://doi.org/10.1016/j.electacta.2012.10.089.
[48] B.W. Gregory, J.L. Stickney, Electrochemical atomic layer epitaxy (ECALE), J. Electroanal. Chem. Interfacial Electrochem. 300 (1991) 543–561, https://doi.org/10.1016/0022-0728(91)85415-L.
[49] R. Vaidyanathan, S.M. Cox, U. Happek, D. Banga, M.K. Mathe, J.L. Stickney, Preliminary Studies in the Electrodeposition of PbSe/PbTe Superlattice Thin Films via Electrochemical Atomic Layer Deposition (ALD), Langmuir 22 (2006) 10590–10595, https://doi.org/10.1021/la061625z.
[50] N. Dimitrov, Recent Advances in the Growth of Metals, Alloys, and Multilayers by Surface Limited Redox Replacement (SLRR) Based Approaches, Electrochim. Acta 209 (2016) 599–622, https://doi.org/10.1016/j.electacta.2016.05.115.
[51] M.F. Mrozek, Y. Xie, M.J. Weaver, Surface-Enhanced Raman Scattering on Uniform Platinum-Group Overlayers: Preparation by Redox Replacement of Underpotential-Deposited Metals on Gold, Anal. Chem. 73 (2001) 5953–5960, https://doi.org/10.1021/ac0106391.
[52] K. Yliniemi, N.T. Nguyen, S. Mohajernia, N. Liu, B.P. Wilson, P. Schmuki, M. Lundström, A direct synthesis of platinum/nickel co-catalysts on titanium dioxide nanotube surface from hydrometallurgical-type process streams, J. Clean. Prod. 201 (2018) 39–48, https://doi.org/10.1016/j.jclepro.2018.08.022.
[53] P.-M. Hannula, S. Pletincx, D. Janas, K. Yliniemi, A. Hubin, M. Lundström, Controlling the deposition of silver and bimetallic silver/copper particles onto a carbon nanotube film by electrodeposition-redox replacement, Surf. Coat. Technol. 374 (2019) 305–316, https://doi.org/10.1016/j.surfcoat.2019.05.085.
[54] Z. Wang, P.-M. Hannula, S. De, B.P. Wilson, J. Vapaavuori, K. Yliniemi, M. Lundström, Controllable Production of Ag/Zn and Ag Particles from Hydrometallurgical Zinc Solutions, ACS Sustain. Chem. Eng. 9 (2021) 8186–8197, https://doi.org/10.1021/acssuschemeng.1c01789.
[55] Z. Wang, K. Yliniemi, E.-L. Rautama, P.-M. Hannula, B.P. Wilson, M. Lundström, Electrochemical Growth of Ag/Zn Alloys from Zinc Process Solutions and Their Dealloying Behavior, ACS Sustain. Chem. Eng. 10 (2022) 3716–3725, https://doi.org/10.1021/acssuschemeng.2c00284.
[56] Z. Wang, K. Yliniemi, B.P. Wilson, M. Lundstöm, Green and Controllable Preparation of Cu/Zn Alloys Using Combined Electrodeposition and Redox Replacement, ACS Sustain. Chem. Eng. 10 (2022) 4770–4779, https://doi.org/10.1021/acssuschemeng.2c00771.
[57] Z. Wang, K. Yliniemi, B.P. Wilson, M. Lundstöm, Targeted surface modification of Cu/Zn/Ag coatings and Ag/Cu particles based on sacrificial element selection by electrodeposition and redox replacement, Surf. Coat. Technol. 441 (2022), 128531, https://doi.org/10.1016/j.surfcoat.2022.128531.
[58] Y.D. Gamburg G. Zangari Theory and Practice of Metal Electrodeposition 2011 Springer New York New York, NY.
[59] A.J. deBethune, T.S. Licht, N. Swendeman, The Temperature Coefficients of Electrode Potentials: The Isothermal and Thermal Coefficients—The Standard Ionic Entropy of Electrochemical Transport of the Hydrogen Ion, J. Electrochem. Soc. 106 (1959) 616–625, https://doi.org/10.1149/1.2427448.
[60] G. Power, I. Ritchie, A contribution to the theory of cementation (metal displacement) reactions, Aust. J. Chem. 29 (1976) 699–709, https://doi.org/10.1071/CH9760699.
[61] J.B. Hiskey, J. Lee, Kinetics of gold cementation on copper in ammoniacal thiosulfate solutions, Hydrometall. 69 (2003) 45–56, https://doi.org/10.1016/S0304-386X(03)00003-3.
[62] M.D. Adams B.A. Wills Advances in Gold Ore Processing M.D. Adams B.A. Wills Developments in Mineral Processing 2005 Elsevier Amsterdam 1 1027.
[63] T. Stefanowicz, M. Osińska, S. Napieralska-Zagozda, Copper recovery by the cementation method, Hydrometall. 47 (1997) 69–90, https://doi.org/10.1016/S0304-386X(97)00036-4.
[64] V. van der Pas, D.B. Dreisinger, A fundamental study of cobalt cementation by zinc dust in the presence of copper and antimony additives, Hydrometall. 43 (1996) 187–205, https://doi.org/10.1016/0304-386X(95)00107-R.
[65] I.M. Ahmed, Y.A. El-Nadi, J.A. Daoud, Cementation of copper from spent copper-pickle sulfate solution by zinc ash, Hydrometall. 110 (2011) 62–66, https://doi.org/10.1016/j.hydromet.2011.08.007.
[66] P.W. Voorhees, The theory of Ostwald ripening, J. Stat. Phys. 38 (1985) 231–252, https://doi.org/10.1007/BF01017860.
[67] E. Bauer, J.H. van der Merwe, Structure and growth of crystalline superlattices: From monolayer to superlattice, Phys. Rev. B 33 (1986) 3657–3671, https://doi.org/10.1103/PhysRevB.33.3657.
[68] S. Ambrozik, N. Dimitrov, The Deposition of Pt via Electroless Surface Limited Redox Replacement, Electrochim. Acta 169 (2015) 248–255, https://doi.org/10.1016/j.electacta.2015.04.043.
[69] M. Fayette, Y. Liu, D. Bertrand, J. Nutariya, N. Vasiljevic, N. Dimitrov, From Au to Pt via Surface Limited Redox Replacement of Pb UPD in One-Cell Configuration, Langmuir 27 (2011) 5650–5658, https://doi.org/10.1021/la200348s.
[70] C.K. Gupta, T.K. Mukherjee, Hydrometallurgy in Extraction Processes, Volume II, first ed., CRC Press, Boca Raton, 1990. https://doi.org/10.1201/9780203751404.
[71] I. Korolev, P. Altinkaya, M. Haapalainen, E. Kolehmainen, K. Yliniemi, M. Lundström, Electro-hydrometallurgical chloride process for selective gold recovery from refractory telluride gold ores: A mini-pilot study, Chem. Eng. J. 429 (2022), 132283, https://doi.org/10.1016/J.CEJ.2021.132283.
[72] Z. Xiu, Q. Zhang, H.L. Puppala, V.L. Colvin, P.J.J. Alvarez, Negligible Particle-Specific Antibacterial Activity of Silver Nanoparticles, Nano Lett. 12 (2012) 4271–4275, https://doi.org/10.1021/nl301934w.
[73] R. Xu, D. Wang, J. Zhang, Y. Li, Shape-Dependent Catalytic Activity of Silver Nanoparticles for the Oxidation of Styrene, Chem. Asian J. 1 (2006) 888–893, https://doi.org/10.1002/asia.200600260.
[74] D.D. Evanoff, G. Chumanov, Synthesis and Optical Properties of Silver Nanoparticles and Arrays, ChemPhysChem 6 (2005) 1221–1231, https://doi.org/10.1002/cphc.200500113.
[75] Y. Li, Y. Wu, B.S. Ong, Facile Synthesis of Silver Nanoparticles Useful for Fabrication of High-Conductivity Elements for Printed Electronics, J. Am. Chem. Soc. 127 (2005) 3266–3267, https://doi.org/10.1021/ja043425k.
[76] F. Liu, J. Wang, C. Peng, Z. Liu, B.P. Wilson, M. Lundström, Recovery and separation of silver and mercury from hazardous zinc refinery residues produced by zinc oxygen pressure leaching, Hydrometall. 185 (2019) 38–45, https://doi.org/10.1016/j.hydromet.2019.01.017.
[77] P.R. Norris, L. Laigle, T.J. Ogden, O.J.P. Gould, Selection of thermophiles for base metal sulfide concentrate leaching, Part I: Effect of temperature on copper concentrate leaching and silver recovery, Miner Eng 106 (2017) 7–12, https://doi.org/10.1016/j.mineng.2016.12.003.
[78] X. Li, Y. Wang, X. Cui, Z. Lou, W. Shan, Y. Xiong, Y. Fan, Recovery of silver from nickel electrolyte using corn stalk-based sulfur-bearing adsorbent, Hydrometall. 176 (2018) 192–200, https://doi.org/10.1016/j.hydromet.2018.01.024.
[79] G. Liu, Y. Wu, A. Tang, D. Pan, B. Li, Recovery of scattered and precious metals from copper anode slime by hydrometallurgy: A review, Hydrometall. 197 (2020), 105460, https://doi.org/10.1016/j.hydromet.2020.105460.
[80] G. Deschênes, Advances in the cyanidation of gold, in: M.D. Adams, B.A. Wills (Eds.), Advances in Gold Ore Processing, Elsevier, Amsterdam, 2005, pp. 479–500, https://doi.org/10.1016/S0167-4528(05)15020-0.
[81] T.M. Sun, W.T. Yen, Kinetics of gold chloride adsorption onto activated carbon, Miner. Eng. 6 (1993) 17–29, https://doi.org/10.1016/0892-6875(93)90160-O.
[82] P. Navarro, C. Vargas, M. Alonso, F. Alguacil, The adsorption of gold on activated carbon from thiosulfate-ammoniacal solutions, Gold Bull. 39 (2006) 93–97, https://doi.org/10.1007/BF03215535.
[83] B. Sayiner, N. Acarkan, Effect of silver, nickel and copper cyanides on gold adsorption on activated carbon in cyanide leach solutions, Physicochem Probl Miner Process 50 (2014) 277–287, https://doi.org/10.5277/mg/lp140123.
[84] E. Jaszczak, Ż. Polkowska, S. Narkowicz, J. Namieśnik, Cyanides in the environment-analysis-problems and challenges, Environ. Sci. Pollut. Res. 24 (2017) 15929–15948, https://doi.org/10.1007/s11356-017-9081-7.
[85] P. Sinisalo, M. Lundström, Refining Approaches in the Platinum Group Metal Processing Value Chain—A Review, Metals 8 (2018) 203, https://doi.org/10.3390/met8040203.
[86] H. Elomaa, L. Rintala, J. Aromaa, M. Lundström, Process simulation based life cycle assessment of cyanide-free refractory gold concentrate processing – Case study: Cupric chloride leaching, Miner. Eng. 157 (2020), 106559, https://doi.org/10.1016/j.mineng.2020.106559.

[87] S. Seisko, J. Aromaa, M. Lundström, Effect of redox potential and OCP in ferric and cupric chloride leaching of gold, Hydrometall. 195 (2020), 105374, https://doi.org/10.1016/j.hydromet.2020.105374.

[88] S. Seisko, J. Aromaa, M. Lundström, Features affecting the cupric chloride leaching of gold, Miner. Eng. 137 (2019) 94–101, https://doi.org/10.1016/j.mineng.2019.03.030.

[89] S. Seisko, M. Lampinen, J. Aromaa, A. Laari, T. Koiranen, M. Lundström, Kinetics and mechanisms of gold dissolution by ferric chloride leaching, Miner. Eng. 115 (2018) 131–141, https://doi.org/10.1016/j.mineng.2017.10.017.

[90] H. Elomaa, M. Leikola, L. Rintala, M. Lundström, Cyanide Free Future of Gold Processing - Process Simulation and Knowledge Modelling, ALTA2019, in, 2019.

[91] G. Kelsall, C.-Y. Cheng, M. Diaz, A. Robson, Gold Electrowinning from Acidic Aqueous Chloride in a Packed Bed Electrode, ECS Trans. 2 (2006) 317–328, https://doi.org/10.1149/1.2196020.

[92] J.O. Marsden C.I. House The Chemistry of Gold Extraction second ed. 2006 Society for Mining Metallurgy, and Exploration, Colorado.

[93] M.J. Nicol C.A. Fleming R.L. Paul The Chemistry of the Extraction of Gold G.G. Stanley The Extractive Metallurgy of Gold in South Africa 1987 South African Institute of Mining and Metallurgy Johannesburg.

[94] M.D. Adams, Gold Ore Processing, second ed., Elsevier, Amsterdam, 2016.

[95] Y. Li, H. Tian, C. Xiao, J. Ding, X. Chen, Efficient recovery of precious metal based on Au–S bond and electrostatic interaction, Green Chem. 16 (2014) 4875–4878, https://doi.org/10.1039/C4GC01375A.

[96] M. Schlesinger, M. King, K. Sole, W. Davenport, Extractive Metallurgy of Copper, fifth ed., Elsevier, Oxford, 2011. https://doi.org/10.1016/C2010-0-64841-3.

[97] J.A. Ober, Mineral Commodity Summaries 2018, U.S, Geological Survey, Reston (2018), https://doi.org/10.3133/70194932.

[98] J. Ibers Tellurium in a twist Nat Chem. 1 2009 508 508 10.1038/nchem.350.

[99] C.B. Murray, D.J. Norris, M.G. Bawendi, Synthesis and characterization of nearly monodisperse CdE (E = sulfur, selenium, tellurium) semiconductor nanocrystallites, J. Am. Chem. Soc. 115 (1993) 8706–8715, https://doi.org/10.1021/ja00072a025.

[100] A. Feltrin, A. Freundlich, Material considerations for terawatt level deployment of photovoltaics, Renew. Energy 33 (2008) 180–185, https://doi.org/10.1016/j.renene.2007.05.024.

[101] G. Kavlak, T.E. Graedel, Global anthropogenic tellurium cycles for 1940–2010, Resour. Conserv. Recycl. 76 (2013) 21–26, https://doi.org/10.1016/j.resconrec.2013.04.007.

[102] V.M. Fthenakis, End-of-life management and recycling of PV modules, Energy Policy 28 (2000) 1051–1058, https://doi.org/10.1016/S0301-4215(00)00091-4.

[103] G. Tang, Q. Qian, X. Wen, G. Zhou, X. Chen, M. Sun, D. Chen, Z. Yang, Phosphate glass-clad tellurium semiconductor core optical fibers, J. Alloy. Compd. 633 (2015) 1–4, https://doi.org/10.1016/j.jallcom.2015.02.007.

[104] Y. Amouyal, On the role of lanthanum substitution defects in reducing lattice thermal conductivity of the AgSbTe2 (P4/mmm) thermoelectric compound for energy conversion applications, Comput. Mater. Sci 78 (2013) 98–103, https://doi.org/10.1016/j.commatsci.2013.05.027.

[105] M. Aspiala, P. Taskinen, Thermodynamic study of the Ag–Sb–Te system with an advanced EMF method, J. Chem. Thermodyn. 93 (2016) 261–266, https://doi.org/10.1016/j.jct.2015.08.025.

[106] J.E. Hoffmann, Recovering selenium and tellurium from copper refinery slimes, JOM 41 (1989) 33–38, https://doi.org/10.1007/BF03220269.

[107] W.D. Bonificio, D.R. Clarke, Bacterial recovery and recycling of tellurium from tellurium-containing compounds by Pseudoalteromonas sp. EPR3, J. Appl. Microbiol. 117 (2014) 1293–1304, https://doi.org/10.1111/jam.12629.

[108] W. Jin, M. Hu, J. Hu, Selective and Efficient Electrochemical Recovery of Dilute Copper and Tellurium from Acidic Chloride Solutions, ACS Sustain. Chem. Eng. 6 (2018) 13378–13384, https://doi.org/10.1021/acssuschemeng.8b03150.

[109] M. Lundström, J. Aromaa, O. Forsén, O. Hyvärinen, M.H. Barker, Leaching of chalcopyrite in cupric chloride solution, Hydrometall. 77 (2005) 89–95, https://doi.org/10.1016/j.hydromet.2004.10.013.

[110] I. Haiduc, R.B. King, M.G. Newton, Stereochemical Aspects of Tellurium Complexes with Sulfur Ligands: Molecular Compounds and Supramolecular Associations, Chem. Rev. 94 (1994) 301–326, https://doi.org/10.1002/chin.199434277.

[111] A.I. Alekperov, Electrochemistry of Selenium and Tellurium, Russ, Chem. Rev. 43 (1974) 235–250, https://doi.org/10.1070/RC1974v043n04ABEH001803.

[112] A.J. Bard R. Parsons J. Jordan . first, Standard Potentials in Aqueous Solution 2017 Routledge New York 10.1201/9780203738764.

[113] G. Broderick, B. Handle, P. Paschen, Strategies for optimal operation of the tellurium electrowinning process, Metall. Mater. Trans. B 30 (1999) 5–13, https://doi.org/10.1007/s11663-999-0001-1.

[114] K.I. Rhee, C.K. Lee, Y.C. Ha, G.J. Jeong, H.S. Kim, H.J. Sohn, Tellurium recovery from cemented tellurium with minimum waste disposal, Hydrometall. 53 (1999) 189–201, https://doi.org/10.1016/S0304-386X(99)00044-4.

[115] B. Handle, G. Broderick, P. Paschen, A statistical response surface study of the tellurium electrowinning process, Hydrometall. 46 (1997) 105–120, https://doi.org/10.1016/S0304-386X(97)00004-2.

[116] T. Shibasaki, K. Abe, H. Takeuchi, Recovery of tellurium from decopperizing leach solution of copper refinery slimes by a fixed bed reactor, Hydrometall. 29 (1992) 399–412, https://doi.org/10.1016/0304-386X(92)90024-T.

[117] Q. Tian, J. Li, X. Guo, D. Li, Y. Yang, Z. Xu, W. Li, Efficient Electrochemical Recovery of Tellurium from Spent Electrolytes by Cyclone Electrowinning, J Sustain Metall 7 (2021) 27–45, https://doi.org/10.1007/s40831-020-00317-z.

[118] Z. Xu, X. Guo, Q. Tian, D. Li, Z. Zhang, L. Zhu, Electrodeposition of tellurium from alkaline solution by cyclone electrowinning, Hydrometall. 193 (2020) 105316.

[119] K. Yliniemi, Z. Wang, I. Korolev, P. Hannula, P. Halli, M. Lundström, Effect of Impurities in Precious Metal Recovery by Electrodeposition-Redox Replacement Method from Industrial Side-Streams and Process Streams, ECS Trans. 85 (2018) 59–67, https://doi.org/10.1149/08504.0059ECST/XML.

[120] V. Stanković, I. Duo, C. Comninellis, F. Zonnevijlle, Silver electrowinning from silver(I)-calixarene complexes by two-phase electrolysis, J. Appl. Electrochem. 37 (2007) 1279–1286, https://doi.org/10.1007/s10800-007-9412-3.

[121] Z. Wang, C. Peng, K. Yliniemi, M. Lundström, Recovery of High-Purity Silver from Spent Silver Oxide Batteries by Sulfuric Acid Leaching and Electrowinning, ACS Sustain. Chem. Eng. 8 (2020) 15573–15583, https://doi.org/10.1021/acssuschemeng.0c04701.

[122] I. Achari, S. Ambrozik, N. Dimitrov, Electrochemical Atomic Layer Deposition of Pd Ultrathin Films by Surface Limited Redox Replacement of Underpotentially Deposited H in a Single Cell, J. Phys. Chem. C 121 (2017) 4404–4411, https://doi.org/10.1021/acs.jpcc.6b12794.

[123] W. Stange, The process design of gold leaching and carbon-in-pulp circuits, J South African Inst Min Metall 99 (1999) 13–26.

[124] I. Korolev, K. Yliniemi, M. Lindgren, L. Carpén, M. Lundström, Performance-Based Selection of the Cathode Material for the Electrodeposition-Redox Replacement Process of Gold Recovery from Chloride Solutions, Metall. Mater. Trans. B 52 (2021) 3107–3119, https://doi.org/10.1007/s11663-021-02239-x.

[125] W. Zhang, G. Houlachi, Electrochemical studies of the performance of different Pb–Ag anodes during and after zinc electrowinning, Hydrometall. 104 (2010) 129–135, https://doi.org/10.1016/j.hydromet.2010.05.007.

[126] Y. Li, L.X. Jiang, X.J. Lv, Y.Q. Lai, H.L. Zhang, J. Li, Y.X. Liu, Oxygen evolution and corrosion behaviors of co-deposited Pb/Pb-MnO2 composite anode for electrowinning of nonferrous metals, Hydrometall. 109 (2011) 252–257, https://doi.org/10.1016/j.hydromet.2011.08.001.

[127] S. Xu, Y. Zhu, D. Xiong, L. Wang, P. Yang, P.K. Chu, Zinc Electrodeposition on Polycrystalline Copper: Electrochemical Study of Early-Stage Growth Mechanism, J. Phys. Chem. C 121 (2017) 3938–3946, https://doi.org/10.1021/acs.jpcc.6b12036.

[128] C. Durante, V. Perazzolo, L. Perini, M. Favaro, G. Granozzi, A. Gennaro, Electrochemical activation of carbon–halogen bonds: Electrocatalysis at silver/copper nanoparticles, Appl Catal B 158–159 (2014) 286–295, https://doi.org/10.1016/j.apcatb.2014.04.023.

[129] V. Mancier, C. Rousse-Bertrand, J. Dille, J. Michel, P. Fricoteaux, Sono and electrochemical synthesis and characterization of copper core–silver shell nanoparticles, Ultrason. Sonochem. 17 (2010) 690–696, https://doi.org/10.1016/j.ultsonch.2009.12.009.

[130] H. Park, J. Choi, H. Kim, E. Hwang, D.-H. Ha, S.H. Ahn, S.-K. Kim, AgIn dendrite catalysts for electrochemical reduction of CO2 to CO, Appl Catal B 219 (2017) 123–131, https://doi.org/10.1016/j.apcatb.2017.07.038.

[131] A. Gomes, A.S. Viana, M.I. da Silva Pereira, Potentiostatic and AFM Morphological Studies of Zn Electrodeposition in the Presence of Surfactants, J. Electrochem. Soc. 154 (2007) D452–D461, https://doi.org/10.1149/1.2752984.

[132] K.I. Popov, N.D. Nikolić, General Theory of Disperse Metal Electrodeposits Formation, in: S.S. Djokić (Ed.), Electrochemical Production of Metal Powders, Springer, Boston, 2012: pp. 1–62. https://doi.org/10.1007/978-1-4614-2380-5_1.

[133] Y. Zuo, K. Wang, P. Pei, M. Wei, X. Liu, Y. Xiao, P. Zhang, Zinc dendrite growth and inhibition strategies, Mater. Today Energy 20 (2021), 100692, https://doi.org/10.1016/j.mtener.2021.100692.

[134] A.A. Rifat, Md. Rabiul Hasan, R. Ahmed, A.E. Miroshnichenko, Microstructured Optical Fiber-Based Plasmonic Sensors, in: M. Hameed, S. Obayya, (Eds.), Computational Photonic Sensors, Springer, Cham, 2019: pp. 203–232. https://doi.org/10.1007/978-3-319-76556-3_9.

[135] M. Cuartero, J. Bishop, R. Walker, R.G. Acres, E. Bakker, R. de Marco, G. A. Crespo, Evidence of double layer/capacitive charging in carbon nanomaterial-based solid contact polymeric ion-selective electrodes, Chem. Commun. 52 (2016) 9703–9706, https://doi.org/10.1039/C6CC04876E.

[136] M. Rinne, H. Elomaa, A. Porvali, M. Lundström, Simulation-based life cycle assessment for hydrometallurgical recycling of mixed LIB and NiMH waste, Resour. Conserv. Recycl. 170 (2021) 105586.

[137] M. Rinne, H. Elomaa, M. Lundström, Life cycle assessment and process simulation of prospective battery-grade cobalt sulfate production from Co-Au ores in Finland, Int. J. Life Cycle Assess. 26 (2021) 2127–2142, https://doi.org/10.1007/s11367-021-01965-3.

[138] M. Rinne, P. Halli, J. Aromaa, M. Lundström, Alternative method for treating electric arc furnace dust: simulation and life cycle assessment, J Sustain Metall 8 (2022) 913–926, https://doi.org/10.1007/s40831-022-00531-x.

[139] M. Rinne, H. Elomaa, S. Seisko, M. Lundstrom, Direct cupric chloride leaching of gold from refractory sulfide ore: process simulation and life cycle assessment, Miner. Process. Extr. Metall. Rev. 43 (2022) 598–609, https://doi.org/10.1080/08827508.2021.1910510.

[140] M.E. Wadsworth, J.D. Miller, Hydrometallurgical Processes, in: H.Y. Sohn, M. E. Wadsworth (Eds.), Rate Processes of Extractive Metallurgy, Springer, Boston, 1979, https://doi.org/10.1007/978-1-4684-9117-3_4.